HHS Public Access

Author manuscript

Hippocampus. Author manuscript; available in PMC 2018 June 19.

Published in final edited form as:

Hippocampus. 2014 November ; 24(11): 1267–1286. doi:10.1002/hipo.22354.

H.M.'s Contributions to Neuroscience: A Review and Autopsy Studies

Jean C. Augustinack[1,#,*], **André J.W. van der Kouwe**[1,#], **David H. Salat**[1], **Thomas Benner**[1], **Allison A. Stevens**[1], **Jacopo Annese**[2], **Bruce Fischl**[1,3], **Matthew P. Frosch**[4], and **Suzanne Corkin**[1,5]

[1]Department of Radiology, Athinoula A. Martinos Center for Biomedical Imaging, Massachusetts General Hospital, Charlestown, Massachusetts

[2]The Brain Observatory, San Diego, California 92101, USA and Department of Radiology, University of California San Diego, San Diego, California 92093, USA

[3]CSAIL, Massachusetts Institute of Technology, Cambridge, Massachusetts

[4]C.S. Kubik Laboratory for Neuropathology, Massachusetts General Hospital, Boston, Massachusetts

[5]Department of Brain and Cognitive Sciences, Massachusetts Institute of Technology, Cambridge, Massachusetts

Abstract

H.M., Henry Molaison, was one of the world's most famous amnesic patients. His amnesia was caused by an experimental brain operation, bilateral medial temporal lobe resection, carried out in 1953 to relieve intractable epilepsy. He died on December 2, 2008, and that night we conducted a wide variety of in situ MRI scans in a 3 T scanner at the Massachusetts General Hospital (Mass General) Athinoula A. Martinos Center for Biomedical Imaging. For the in situ experiments, we acquired a full set of standard clinical scans, 1 mm isotropic anatomical scans, and multiple averages of 440 μm isotropic anatomical scans. The next morning, H.M.'s body was transported to the Mass General Morgue for autopsy. The photographs taken at that time provided the first documentation of H.M.'s lesions in his physical brain. After tissue fixation, we obtained ex vivo structural data at ultra-high resolution using 3 T and 7 T magnets. For the ex vivo acquisitions, the highest resolution images were 210 μm isotropic. Based on the MRI data, the anatomical areas removed during H.M.'s experimental operation were the medial temporopolar cortex, piriform cortex, virtually all of the entorhinal cortex, most of the perirhinal cortex and subiculum, the amygdala (except parts of the dorsal-most nuclei—central and medial), anterior half of the hippocampus, and the dentate gyrus (posterior head and body). The posterior parahippocampal gyrus and medial temporal stem were partially damaged. Spared medial temporal lobe tissue included the dorsal-most amygdala, the hippocampal-amygdalotransition- area, ~2 cm of the tail of the hippocampus, a small part of perirhinal cortex, a small portion of medial hippocampal tissue, and ~2 cm of posterior parahippocampal gyrus. H.M.'s impact on the field of memory has

[*]Correspondence to: Jean C. Augustinack, 149, 13th St., Room 2301, Charlestown, MA 02129, USA. jean@nmr.mgh.harvard.edu.

[#]J.C.A. and A.J.W.V.D.K. contributed equally to this work.

been remarkable, and his contributions to neuroscience continue with a unique dataset that includes in vivo, in situ, and ex vivo high-resolution MRI.

Keywords

hippocampus; entorhinal cortex; perirhinal cortex; parahippocampal cortex; amygdala

INTRODUCTION

This review chronicles H.M.'s history, his contributions to the neuroscience of memory, neuroimaging studies past and present, and his autopsy. In the following paragraphs, we walk through the anatomical details of the medial temporal lobe, describe the specific structures removed and spared in H.M., and provide the only glimpse of his intact, fresh brain. We recount the critical discoveries that made him one of the most famous amnesic patients in the world, and illustrate, with high-resolution imaging, the age-related white matter disease that likely accounts for his dementia in the final part of his life. We also identify key questions to be addressed in the forthcoming neuropathological examination and in future histological studies.

On August 25, 1953, the neurosurgeon William Beecher Scoville performed an experimental operation in a 27-year-old man, Henry Gustave Molaison (H.M.), in the hope of curing his medically intractable epilepsy (Scoville, 1954; Scoville and Milner, 1957). H.M. had experienced petit mal seizures from the age of 10 and grand mal seizures that began on his 15th birthday. The etiology of his seizures was unclear—as a young boy, he had sustained a minor head injury and, in addition, several of his father's relatives had epilepsy. H.M. graduated from high school when he was 21 and later repaired electric motors and worked on a typewriter assembly line. He took large doses of anti-epilepsy drugs, but they did not quell his attacks. Because numerous EEG studies failed to reveal a precise surgical target for seizure control, Scoville proposed a psychosurgical procedure that he had devised, bilateral medial temporal lobotomy (Scoville and Milner, 1957). He had previously performed the operation in patients with psychiatric disorders, mainly schizophrenia, with mixed results. H.M. was the first patient to undergo this procedure for intractable epilepsy. Scoville later renamed the operation bilateral medial temporal lobe resection.

Postoperatively, H.M.'s petit and grand mal attacks continued, and although their frequency decreased markedly, he required anti-epilepsy drugs for the rest of his life. His seizure control, however, was accompanied by a devastating loss. For the next 55 years, H.M. was trapped in the moment because of profound anterograde amnesia. His amnesia was pure—unconfounded by other cognitive deficits. His IQ was above average, and his language, reasoning, and perceptual capacities were normal. The exceptions were impaired olfactory function, caused by the operation, and cerebellar symptoms, a side effect of his anti-seizure medication, Dilantin.

The discrete nature and severity of H.M.'s amnesia made him the topic of scientific scrutiny for the remainder of his life and even after his death. Over 100 researchers participated in collaborative projects to study him, integrating behavioral testing, standardized interviews,

and structural and functional imaging. In 1955, Brenda Milner conducted the first postoperative psychological testing of H.M., providing quantitative evidence of profound memory loss with preserved intelligence and immediate memory (Scoville and Milner, 1957). She and Scoville concluded, “The findings reported herein have led us to attribute a special importance to the anterior hippocampus and hippocampal gyrus in the retention of new experience” (p. 21). Milner later introduced the idea that some memory processes were not hippocampus dependent by showing that H.M.’s error scores decreased across three days of testing on a motor skill-learning task, mirror tracing (Milner, 1962). This discovery constituted the first experimental demonstration of preserved learning in amnesia.

Dissociable Memory Processes

Subsequent research with H.M. extended Milner’s pioneering work and established several firm conclusions. The evidence supported the dual process theory of memory proposed by James (1890) and Hebb (1949). They viewed short-term and long-term memory as separate processes. Accordingly, H.M.’s short-term memory was preserved, while his long-term memory was impaired. His episodic and semantic learning were both deficient, indicating overlapping neural substrates (Gabrieli et al., 1988; Steinvorth et al., 2005). Tests that distinguished two forms of recognition memory—recollection and familiarity—revealed that H.M. could make familiarity-based judgments to recognize complex pictures, even six months after encoding. This surprising result showed that recollection depends on the hippocampus, but familiarity does not. Examinations of H.M.’s retrograde amnesia led to the discovery that he could remember only two preoperatively experienced autobiographical episodes, whereas his semantic memory for the same time period was normal (Steinvorth et al., 2005; Corkin, 2013). This dissociation implicates the hippocampus as necessary for the retrieval of premorbid autobiographical but not semantic information. At the same time, certain kinds of nondeclarative learning—motor skill learning, classical conditioning, and repetition priming—were preserved.

The issues that motivated decades of research with H.M. were to understand the scope of his amnesia, to elucidate the kinds of learning and memory that were spared, and to establish a causal link between his amnesia and specific brain circuits. Some information about the integrity of his brain was available even before his operation. H.M. had a pneumoencephalogram in 1946 and another in 1953, both of which were read as normal. At the time of his operation in 1953, information about the damage to his brain came exclusively from Scoville’s account of what he had removed. His notes and drawings formed the basis of a set of detailed drawings by another neurosurgeon, Lamar Roberts, which accompanied Scoville and Milner’s 1957 paper (Scoville and Milner, 1957). Scoville estimated that the medial temporal lobe resection extended 8 cm back from the tip of each temporal lobe, but subsequent MRI scans indicated that the removal was much less extensive.

Postoperative In Vivo Imaging

CT scans carried out in 1977 and 1984 showed metallic clips from the operation, minimal atrophic change in the anterior temporal region bilaterally, cerebellar atrophy, and, in the 1984 scan when he was 58, mild to moderate cortical atrophy (Corkin, 1984). Specific brain

structures were not visualized. A SPECT scan conducted in 1992 at Brigham and Women's Hospital in Boston confirmed his bilateral medial temporal lobe resection and cerebellar atrophy.

H.M.'s first MRI scans occurred in 1992 at Brigham and Women's Hospital and in 1993 at Mass General, when he was 66 and 67 years old, respectively (Corkin et al., 1997). These images showed that the removal extended back about 5.4 cm from the tip of the temporal lobe on the left and about 5.1 cm on the right. The bilaterally symmetrical lesion damaged most of the amygdaloid complex, the entorhinal cortex, part of perirhinal cortex, the uncal and rostral portions of the hippocampal complex, and part of parahippocampal cortex. Some of the ventral perirhinal and posterior parahippocampal cortices were intact. Approximately 2 cm of caudal hippocampal tissue was also spared, but it appeared atrophic and was likely deafferented due to removal of the entorhinal cortex. The subcortical white matter associated with the most anterior portions of the superior, middle, and inferior temporal gyri may have been compromised by the resection. The cerebellar atrophy was dramatic, but the cortical surface appeared normal for H.M.'s age (Corkin et al., 1997).

A decade later, in 2002 to 2004, Salat and colleagues scanned H.M. at the Mass General Martinos Center, using improved MRI data acquisition and analysis tools—higher resolution, quantitative measures of tissue morphometry, and indices of tissue integrity (Salat et al., 2004, 2006; van der Kouwe et al., 2005, 2006; Wiggins et al., 2006). By then, H.M. was 74 to 77 years old, and we uncovered new age-related abnormalities that were not connected to his 1953 resection—cortical thinning and abnormal signal in white matter and deep gray matter. H.M.'s T1 morphometry images showed significant atrophy of the cerebral ribbon, ranging from ~0.3 mm to ~0.7 mm relative to control participants. The atrophy that occurred between 1998 and 2003 was greater than that between 1993 and 1998, suggesting an aging-related degenerative process (Salat et al., 2006). T1-weighted images also revealed infarcts in a number of subcortical gray matter structures, including the thalamus and putamen. Consistent with earlier imaging studies, H.M.'s cerebellum was severely atrophied. In T2-weighted images, Salat et al. noted significant white matter hyperintensities throughout H.M.'s brain that were especially pronounced in the inferior frontal gyrus near the corpus callosum. These new abnormalities appeared to be the result of high blood pressure and small vessel disease. We also collected the first diffusion MRI scans of H.M.'s brain, allowing the examination of fractional anisotropy (FA) maps to quantify the microstructural integrity of the white matter. Overall, H.M. had decreased FA compared to matched controls, and the focal areas of white matter damage had reduced FA. We never found any abnormality that would account for his original seizure disorder.

Current Study

H.M. died on December 2, 2008. That night, we conducted a wide variety of in situ MRI scans in a 3 T scanner at the Mass General Athinoula A. Martinos Center for Biomedical Imaging. The next morning, H.M.'s body was transported to the Mass General Morgue where Matthew Frosch, Director of the Neuropathology Unit, performed an autopsy. Jacopo Annese assisted with the autopsy. Photographs taken immediately afterward provided the first documentation of H.M.'s lesions in his physical brain. After ~10 weeks of tissue

fixation, we obtained ex vivo structural data at ultra-high resolution using 3 T and 7 T magnets. This postmortem research had two goals—to document the specific structures that were removed and spared in H.M.'s brain, based on the gross examination of the fresh brain and analysis of the MRI images, and to relate the behavioral dissociations documented during H.M.'s life to the precisely established sparing and loss of brain tissue. An additional motivation for the ex vivo imaging was to provide an MRI-based method to later register the histological sections in 3D. The Partners Human Research Committee approved all studies described here. In this report, we first introduce the anatomical structures that define the medial temporal lobe region and then describe H.M.'s autopsy and MRI results.

MATERIALS AND METHODS

Participant, H.M

At the time of his death, H.M. was 82 years old. The cause of death was arteriosclerotic cardiovascular disease. In 1992, H.M. and his court-appointed conservator had signed a brain donation form authorizing Mass General and MIT to perform a postmortem examination upon his death, and the conservator gave consent for the autopsy the evening H.M. died.

Neuroanatomy of the Intact Adult Medial Temporal Lobe—Terminology

To establish the terminology used in this report, we first describe pertinent structures in an intact adult brain, focusing on the medial temporal lobe region (Rosene and Van Hoesen, 1987; Gloor, 1995; Insausti et al., 1995; Van Hoesen, 1995; Insausti et al., 1998). To educate the reader on the relevant structures, we selected nine blockface images from a control case (60 year old, male) in our MGH brain collection and labeled them (Fig. 1). The areas include the piriform cortex (primary olfactory cortex), mesocortices of the parahippocampal gyrus (entorhinal and perirhinal cortices), and temporal polar cortex; the hippocampal formation—hippocampus, subiculum, and dentate gyrus; and the subcortical collection of nuclei that comprise the amygdala (Fig. 1). The structures and slices are described from anterior to posterior.

The temporal pole is divided into four regions: dorsal, ventral, medial, and lateral. Anteriorly, the temporal polar cortex hangs unattached to other brain tissue for ~1.5 cm (Fig. 1A), after which the temporal lobe joins the frontal cortex at the level of the limen insula. At this level, several features are noteworthy. The frontal insula and temporal insula merge together, the temporal polar cortex ends, and the piriform cortex begins to occupy the medial temporal area (Fig. 1B). The sulcal configuration in this region is complicated because the rhinal sulcus is incipient in humans and not present in all brains. The main sulci that outline the parahippocampal gyrus include the rhinal sulcus anteriorly, albeit variably, and the collateral sulcus laterally. The control case illustrated in Figure 1 does not exhibit a rhinal sulcus. If a rhinal sulcus were present, it would reside approximately at level B, at the level of the piriform cortex. Deep to the parahippocampal gyrus, the endorhinal sulcus dorsally separates the corticomedial nuclei of the amygdala from the optic tract area, the sulcus semi-annularis separates the medial parahippocampal cortex from the corticoamygdala-transition-area, and the hippocampal fissure separates the parahippocampal gyrus from the

hippocampus (Figs. 1C–F). At the point where the frontal and temporal lobar regions connect, the temporal stem, one of the major white matter conduits for the temporal lobe, appears.

The amygdala lies posterior and slightly dorsal to the piriform cortex, which is situated deep beneath the parahippocampal cortex between the olfactory cortex anteriorly and the hippocampus posteriorly. The key amygdala nuclei are (from lateral to medial) the lateral nucleus, basal nucleus, accessory basal nucleus, paralaminar nucleus, medial nucleus, cortical nucleus, and corticoamygdala-transition-area (Figs. 1C,D). At the medial most edge of the amygdala, three nuclei line up from superior to inferior: medial nucleus, cortical nucleus, and corticoamygdala-transition area (Figs. 1C,D).

At the amygdala's broadest part, immediately anterior and slightly dorsal to the hippocampus, the parahippocampal gyrus is also at its largest width. The anterior parahippocampal gyrus contains two Brodmann areas, area 34 medially and area 28 laterally (Brodmann, 1909; Lorente de No, 1934). Brodmann area 34 corresponds to the gyrus ambiens and sometimes has a bulbar configuration that is often mistaken for the uncus of the hippocampus, but the uncus resides deep to the gyrus ambiens and slightly posterior (Fig. 1D). The hippocampal fissure borders the uncus and lower bank of the parahippocampal gyrus where the subicular cortices are located (Fig. 1E). Brodmann area 28 makes up a substantial component of the parahippocampal territory and occupies the entire crown of the anterior parahippocampal gyrus, commonly referred to as the entorhinal cortex. Equally prominent within the parahippocampal cortex is the entorhinal cortex's neighbor laterally, the perirhinal cortex (Figs. 1B–I). The perirhinal cortex (Brodmann area 35, Braak's transentorhinal) (Braak and Braak, 1985) is sometimes slightly larger than the entorhinal cortex and surrounds it anteriorly, laterally, and posteriorly (Insausti et al., 1998; Van Hoesen et al., 2000; Ding and Van Hoesen, 2010). The perirhinal cortex lies lateral to the rhinal sulcus but medial relative to the collateral sulcus, once the collateral sulcus has begun (Van Hoesen et al., 2000; Ding et al., 2009). The ectorhinal cortex (Brodmann area 36) is temporal isocortex; we classify it separately from perirhinal cortex based on the fact that perirhinal area 35 is agranular and dysgranular (area 35a periallocortex and 35b proisocortex, respectively), whereas temporal isocortex (area 36) contains a granular layer. On the crown of the posterior parahippocampal gyrus, areas TH and TF (von Economo and Koskinas, 1925; von Bonin and Bailey, 1947) make up the remaining parahippocampal cortex as it ends caudally at the retrosplenial cortex and calcarine sulcus (TH-TF, not illustrated).

The hippocampal formation comprises the hippocampus proper, subicular cortices (subiculum, presubiculum, and parasubiculum), and dentate gyrus (Rosene and van Hoesen, 1987). The hippocampus proper contains subfields CA1, CA2, CA3, and CA4, named for cornu ammonis because it resembles a ram's horn. The hippocampus, which contains four main structural parts, genu (Fig. 1D), head (Figs. 1E–G), body (Figs. 1G–I), and tail (not illustrated), sits deep beneath the parahippocampal cortex. Its structure changes significantly from anterior to posterior, with the head being disproportionately larger than the body and tail. The head of the hippocampus is made up of several convolutions, the pes hippocampi, where the medial-most convolution defines the uncus (Figs. 1E,F). The inferior horn of the

lateral ventricle makes its first appearance at the level of the amygdala and hippocampal head.

Autopsy and Fixation

On December 4, 2008, when the postmortem interval was ~19 hrs, Matthew Frosch conducted the autopsy. H.M.'s brain was fixed in standard 10% formalin for several hours and was then transferred to buffered 4% paraformaldehyde. The fixative solution was changed twice during the two months that it remained in the Mass General Department of Pathology, allowing the brain tissue to fix thoroughly. On February 12, 2009, when it was transferred to the Martinos Center for ex vivo scanning, it remained in 4% paraformaldehyde.

In Situ MRI Acquisition

On the evening of December 2, 2008, just under 4 hr after H.M.'s death in Windsor Locks, Connecticut, we collected in situ scans at the Mass General Martinos Center. In situ refers here to postmortem imaging of the brain in the head. Images were collected in a 3 T Siemens (Erlangen, Germany) TIM Trio MRI scanner with a 32-channel head coil. We determined beforehand that the configuration of this system (in particular, the imaging gradient switching and RF energy deposition) would not damage the brain by heating the tissue or by heating or vibrating the surgical clips.

Because subject fatigue and motion were not an issue and scanning could continue for several hours, we collected high-quality, high-resolution images that would not be possible in a living subject. The in situ 3 T session lasted 9 hr. We obtained a wide range of contrasts of the unfixed brain with different scan types and high-resolution anatomical images.

We first acquired a full set of standard clinical scans for comparison with antemortem images. In addition, we obtained a 2 mm isotropic diffusion scan, 1 mm isotropic single and multiecho MPRAGEs (Mugler and Brookeman, 1990; van der Kouwe et al., 2008), 1 mm isotropic multi-flip angle multiecho FLASH scans with 2 mm isotropic B1± maps, and multiple averages of a 440 μm isotropic single-echo multi-flip angle FLASH scan. All scans were automatically localized for acquisition using AutoAlign (van der Kouwe et al., 2005; Benner et al., 2006). The synthetic images presented in this report were generated using estimates of intrinsic tissue parameters derived from a combination of acquired multiecho FLASH images with native contrast (Fischl et al., 2004).

Clinical scans—We obtained five standard clinical scans: (1) sagittal T1-weighted spin-echo, (2) axial T2-weighted turbo-spin-echo, (3) axial FLAIR, (4) susceptibility weighted imaging (SWI), and (5) diffusion with matching B0 field map. Prescan intensity normalization was applied to all scans.

- T1-weighted 2D-encoded spin-echo (T_{acq} 4 m 20 s); 24 sagittal slices of 5 mm with 1 mm gap, 240 mm field of view with 256 matrix and 75% phase resolution, phase encode AP (1.3 × 0.9 × 5 mm). TE 7.1 ms, TR 550 ms, BW 201 Hz/px, FA 120°, two concatenations.

- T2-weighted 2D-encoded turbo-spin-echo (T_{acq} 5 m 27 s); 23 axial slices of 5 mm with 1 mm gap, 230 × 172.5 mm field of view with 512 matrix and 75% phase resolution, phase encode RL (0.6 × 0.4 × 5 mm). TE 91 ms, TR 5 s, BW 100 Hz/px, FA 134°, two averages, flow compensation in slice direction.
- FLAIR 2D-encoded turbo-spin-echo (T_{acq} 6 m 52 s); 23 axial slices of 5 mm with 1 mm gap, 230 × 172.5 mm field of view with 384 matrix and 75% phase resolution, phase encode RL (0.8 × 0.6 × 5 mm). TE 71 ms, TR 10 s, TI 2,500 ms, BW 130 Hz/px, FA 150°, two averages, flow compensation in slice direction.
- Susceptibility-weighted 3D-encoded gradient echo (T_{acq} 6 m 59 s). 96 axial partitions (k-space slices) of 1.5 mm, 220 × 171.9 mm field of view with 448 × 350 matrix, phase encode RL (0.5 × 0.5 × 1.5 mm). TE 20 ms, TR 28 ms, BW 120 Hz/px, FA 15° (slab-selective), flow compensation.

Standard anatomical scans for morphometry—We collected a standard set of 1 mm isotropic anatomical scans designed to elucidate brain morphometry using FreeSurfer (http://surfer.nmr.mgh.harvard.edu) (Dale et al., 1999; Fischl et al., 2002, 2004). The set consisted of T1-weighted multiecho MPRAGE (MEMPR) for cortical modeling and subcortical segmentation, multiecho FLASH (MEF) for tissue parameter quantification, and T2-SPACE and FLAIR T2-SPACE for T2 contrast. Prescan normalization was applied to all scans, and, for accurate alignment, scans were matched with respect to geometry and bandwidth (thus, degree of distortion).

- T1-weighted 3D-encoded 4-echo MEMPR (van der Kouwe et al., 2008) (T_{acq} 6 m 3 s); 176 sagittal partitions of 1 mm, 256 mm field of view with 256 × 256 matrix, phase encode AP (1 mm isotropic), 2× GRAPPA with 32 reference lines. TE 1.64/3.5/5.36/7.22 ms, TR 2,530 ms, TI 1,200 ms (non-selective), BW 651 Hz/px, FA 7° (nonselective).
- T1-weighted 3D-encoded 8-echo FLASH (T_{acq} 13 m 25 s at each of three flip angles); 176 sagittal partitions of 1 mm, 256 mm field of view with 256 × 256 matrix, phase encode AP, 50% phase oversampling (1 mm isotropic), 2× GRAPPA with 32 reference lines. TE ($1.85 + n \times 2.0 + n \times (n–1)/2 \times 0.1$) ms ($n$ = 0,…,7) (uneven spacing for phase unwrapping), TR 22 ms, BW 651 Hz/px, FA 5/20/30° (nonselective), magnitude and phase images.
- T2-weighted variable flip angle 3D-encoded turbo-spin-echo (T2-SPACE) (Mugler et al., 2000) (T_{acq} 4 m 43 s); 176 sagittal partitions of 1 mm, 192 mm field of view with 192 × 192 matrix, phase encode AP (1 mm isotropic), 2× GRAPPA with 24 reference lines. TE 368 ms, TR 3,200 ms, BW 651 Hz/px, FA variable (nonselective).
- T2-weighted variable flip angle 3D-encoded turbo-spin-echo with fluid attenuation (FLAIR T2-SPACE) (Mugler et al., 2000) (T_{acq} 7 m 22 s). 176 sagittal partitions of 1 mm, 192 mm field of view with 192 × 192 matrix, phase encode AP (1 mm isotropic), 2× GRAPPA with 24 reference lines. TE 352 ms, TR 5 s, TI 1,800 ms, BW 789 Hz/px, FA variable (nonselective).

T2*-weighted anatomical scans—To quantify tissue T2*, we carried out a multiecho FLASH scan according to a protocol that had a longer TR and more widely spaced echoes than the 8-echo FLASH described above. We also repeated the 8-echo FLASH protocol at 2 mm isotropic resolution (two repetitions of T_{acq} 6 m 42 s with 128 × 128 matrix).

- 3D-encoded 8-echo FLASH (T_{acq} 14 m 15 s). 128 sagittal partitions of 1.33 mm, 256 mm field of view with 192 × 192 matrix, phase encode AP (1.33 mm isotropic), 2× GRAPPA with 32 reference lines. TE ($3.41 + n \times 6.9 + n \times (n - 1)/2 \times 0.1$) ms ($n = 0,.,7$) (uneven spacing for phase unwrapping), TR 60 ms, BW 202 Hz/px, FA 20° (nonselective), magnitude and phase images.

High-resolution anatomical scans—We dedicated ~5 hr of the in situ scanning time to obtaining high-resolution anatomical scans, using a single-echo FLASH protocol with an isotropic resolution of 440 μm.

- T1-weighted 3D-encoded FLASH (T_{acq} 24 m 19 s at each of 6 flip angles); 384 sagittal partitions of 0.44 mm, 225 mm field of view with 512 × 512 matrix, phase encode AP, 50% phase oversampling (1 mm isotropic), 2× GRAPPA with 32 reference lines. TE 4.09 ms, TR 9.5 ms, BW 199 Hz/px, FA 3/5/8/10/15/18° (non-selective), magnitude and phase images.

Quality control scans—We obtained additional scans to correct artifacts. For the diffusion scans, matching B0 field maps were acquired. We collected data for 1 mm isotropic DESPOT1, DESPOT2, and HiFi analyses (Deoni et al., 2003, 2005; Deoni, 2007). Based on these results, we chose the optimal range of flip angles for the subsequent FLASH scans. We obtained a B1 transmit map using Actual Flip Angle Imaging (Yarnykh, 2007) at 2.5 mm isotropic resolution and a B1 transmit/receive map by imaging at 2 mm isotropic resolution with the body coil and with each element of the 32-channel array. In addition, we acquired a gradient echo EPI series of volumes (TR 3 s, 192 measurements, 3 mm resolution with 0.6 mm gap between slices, 42 slices). Two additional runs used an experimental radial and Cartesian-encoded gradient echo protocol with an ultrashort echo (FLUSTER) (Van der Kouwe, 2008) (data not shown).

Ex Vivo Imaging

Ex vivo imaging occurred after H.M.'s brain had been stored in 10% formalin for ~10 weeks. The fixed brain was placed in a custom-made Plexiglas chamber and imaged at high field (Annese et al., 2014). We repeated the in situ scans ex vivo, and as expected the images confirmed the observations made in in situ.

High-resolution scans (7 T)—We used a 7 T Siemens scanner based on the Avanto platform for high-resolution imaging with a 31-channel custom-built head coil. The highest resolution images were 210 μm isotropic single-echo multi-flip angle FLASH scans. We measured coil covariance for image reconstruction and obtained 1.68 mm isotropic B1 transmit/receive maps and a two-echo gradient echo field map (2 mm × 2 mm × 3 mm resolution) for image correction.

We dedicated 15.5 hr of scan time to collecting high-resolution images of the entire fixed brain. Encoding at 210 μm isotropic resolution with the 31-channel head coil required offline image reconstruction because the k-space data volumes were larger than the 32 GB of RAM available on the scanner image reconstruction computer. The *k*-space data were streamed to an external storage site during acquisition because the total amount of data per scan exceeded the 320 GB of disk space available on the scanner RAID. We used the coil covariance matrix to combine the signals from the 31 head coil channels to form a single image volume (Roemer et al., 1990).

- T1-weighted 3D-encoded FLASH (T_{acq} 4 h 50 m at each of three flip angles); 704 partitions of 210 μm, 175 × 153 mm field of view with 832 × 728 matrix (210 μm isotropic). TE 15.1 ms, TR 34 ms, BW 40 Hz/px, FA 10/20/30° (nonselective).

Temperature Monitoring

From the time of H.M.'s death until his body reached the Martinos Center, his head was enclosed in a Cryopak Ice Blanket to keep his brain cool. During the in situ scanning, room temperature was maintained at ~18°C. During ex vivo scanning, we monitored temperature carefully, keeping it below 19°C on the outer surface of the chamber at 3 T and 7 T. Temperature was a concern because RF energy deposition during MR imaging can heat the sample. To ensure that temperature fluctuations due to imaging would be well below normal fluctuations in room temperature, we previously monitored a test sample (whole brain) during imaging with the highest specific absorption rate sequences. A multichannel fiber optic temperature sensor (Neoptix, Inc., Quebec, Canada) recorded the temperature in four areas—deep in the tissue, close to the inner wall of the chamber, on the outer surface of the chamber, and in the room air. As expected, even during high (100%) specific absorption rate protocols, the temperature inside the tissue never increased more than 4°C relative to the inside and outside of the container. The specific absorption rate of RF energy for the 3 T diffusion sequence was close to 100% of the clinically safe value imposed by the scanner hardware, and it was substantially lower for the other protocols. The room temperature was at the minimum thermostat setting (18°C), and an additional fan was used to dissipate heat from around the chamber. The temperatures of the outer surface of the chamber and the surrounding air were monitored with the fiber optic system. Because these temperatures never exceeded 19°C, we reasoned that the temperature of the brain tissue never went above 23°C during imaging. We believe that the temperature differentials were even smaller during in situ imaging because the imaging session was shorter, the protocols were less energy intensive, and the energy could dissipate throughout the body.

RESULTS

Lesions in the Fresh

Brain The unfixed brain weighed 1,100 g, ~200 g less than one would expect for a 6-foot-tall, healthy man. Photographs of the brain taken immediately after its removal from the skull showed the overall topography of the gross brain to be relatively preserved. Notably, the olfactory bulbs and tracts were intact, and we saw no explicit damage, with the obvious

exceptions of the medial temporal lobe excisions and a shriveled cerebellum (Fig. 2). The dashed white lines drawn laterally and posteriorly illustrate where a normal sized cerebellum would be. The blood vessels appeared mildly atherosclerotic. In the right ventral temporal lobe, we identified a black surgical clip, which we believe was intentionally left behind by Scoville to prevent bleeding (Scoville and Milner, 1957). A second clip was located in the left temporal lobe.

Figure 3 magnifies the ventromedial view to reveal a close-up of the right (A) and left (B) medial temporal lobe lesions. The photographs show slightly different views, a consequence of the unfixed state. (An unfixed brain collapses or widens slightly and does not retain the classical formation until fixed.) The medial temporal lobe lesions began immediately to the left and right of the optic nerves, which had been cut during the autopsy so the brain could be pulled out of the skull, leaving the eyes intact. On both sides, the lesion extended posteriorly from the temporal polar cortex through the parahippocampal gyrus until about the level of the halfway point of the basilar artery. In a normal case, the gyrus ambiens would reside immediately and slightly anterior to the uncus. In H.M., medial tissue remained on both sides but to a greater extent on the left (Figs. 3A,B). We could not determine definitively whether the remaining medial tissue on the left was uncus or gyrus ambiens because the banks of the hippocampal fissure and other landmarks had been surgically removed. The histological analysis, which will be the topic of a later report, will reveal whether the cytoarchitecture of this tissue is hippocampal (allocortical) or cortical (periallocortical). Continuing posteriorly, significant scar tissue occupied the medial temporal areas bilaterally.

In Situ MRI

The several different contrasts acquired in situ provided an MEMPR (T1-weighted) image (Fig. 4A) with the classic MRI contrast that shows CSF as dark and white matter as white. In the T2-SPACE acquisition (Fig. 4B), white matter was relatively dark, gray matter was brighter, and CSF was brightest. Because the lesion void was filled with CSF, it appeared bright in the image. In the T2-SPACE acquisition with fluid attenuation (FLAIR) (Fig. 4C), the CSF in the region of the lesion was dark, but the remaining tissue fragments were relatively bright and clearest compared to other contrasts. The bottom panels of Figure 4 show quantitative proton density (PD) (Fig. 4D) and T1 estimates (Fig. 4E) together with a synthetic image constructed from the corresponding 440 μm volumes (Fig. 4F) (Fischl et al., 2004). We estimated the T1 and PD volumes from a combination of multiecho FLASH scans with different flip angles. Figure 4D shows only PD contrast (arbitrary units, but proportional to spin density); Figure 4E shows estimated T1 relaxation time (sec). PD reflected only the proton (or spin) density and was a relatively flat contrast. The lesions appeared fairly bright because CSF is relatively dense in free water, while the PD of white matter is slightly less than that of gray matter. Both appeared darker than CSF in the PD image. Because higher T1 produces darker voxels in T1-weighted images, the image showing the absolute T1 value had the opposite contrast of the MEMPR (i.e., white matter is darker than gray matter and CSF in the quantitative image because white matter has a shorter T1 relaxation time). To optimize contrast and increase signal-to-noise, we created a synthetic image from the FLASH scans (Deoni et al., 2003; Fischl et al., 2004). Figure 4F shows the

synthetic FLASH image that would result if the TR had been 22 ms, flip angle had been 20°, and TE had been 0. This image was synthesized from the PD and T1 estimates by applying the steady-state FLASH model, in the reverse of the estimation procedure. We chose the TR and flip angle to achieve optimal discrimination between the structures segmented by FreeSurfer (http://www.surfer.nmr.mgh.harvard.edu/), based on contrast (TE 0 implies no signal decay due to T2* relaxation). The synthetic image in Figure 4F has a T1-weighted contrast similar to the MPRAGE.

Lesions in medial temporal lobe structures—Here we describe the specific medial temporal lobe areas that were explicitly removed and identify other structures that remained. The 12 coronal MR images (Fig. 5) highlight the lesion extent and illustrate remaining anatomical structures, based on remaining landmarks (Figs. 5A–L). Levels are spaced 4 mm apart. The first image shows the temporal pole where the anterior-most portion of the lesion began (Fig. 5A). The medial temporopolar cortex, mainly dysgranular area 38 and area 36, were removed. The temporal polar sulcus, located dorsally, was partially destroyed.

In the second image (Fig. 5B), the lesion entered prime temporal polar cortex territory, where we observed the optic nerves (slightly off the midline) and the caudate nucleus. Here, the limen insula had not yet connected to the frontal and temporal lobes. The temporal polar areas, 38 and area 36, were still absent at this level. The olfactory tract, seen inferiorly to the orbitofrontal gyrus, appeared normal. The third image (Fig. 5C) was approximately at the level of the anterior amygdala.

The fourth image (Fig. 5D) fell at the level of the optic chiasm. Presumptive medial structures were the posterior piriform cortex, part of perirhinal cortex (area 35), and temporal isocortical area 36. In all slices described thus far, the medial temporal stem was partially damaged bilaterally, and the white matter quality appeared compromised, with the lesion in the left hemisphere extending farther medially than in the right. The collateral sulcus appeared in images four through eight (Figs. 5D–H), and perirhinal cortex occupied its medial bank.

A small part of the entorhinal cortex appeared in the fifth and sixth images (Figs. 5E,F), but only on the extreme lateral convexity of the gyrus. The border between the entorhinal and perirhinal cortices typically falls on the corner of the parahippocampal gyrus near the collateral sulcus. The fifth image captured the emerging optic tracts, anterior commissure (midline), and caudate/putamen (Fig. 5E). The anterior-most amygdala—specifically parts of the endopiriform nucleus and the corticoamygdalo-transition-area—might have been present in this image. Noticeably, the anterior-amygdala-area was lacking at this level. The landmarks in the sixth image included the optic tract, anterior commissure laterally (very subtle), caudate/putamen/anterior limb of the internal capsule, globus pallidus, hypothalamus, and columns of the fornix, indicating that this slice was at the level of the mid-amygdala (Fig. 5F). In a healthy brain, this level would represent the amygdala at its largest extent along with the gyrus ambiens (Brodmann area 34 in humans). The left side may have contained a portion of the semilunar gyrus slightly dorsal to gyrus ambiens; this possibility will be examined in the histological analysis. Figure 5F shows the best MRI example of the medial tissue that remained. The hypothalamus appeared atrophied, likely

due to the lack of hippocampal input, and the fornix and hippocampal commissure showed significant atrophy.

The seventh image is where one would expect to see the posterior amygdala, subiculum, and anterior-most hippocampus, given that other landmarks usually present at this level are visible—the mammillary bodies of the hypothalamus, the thalamus, putamen, globus pallidus, and the optic tract (tucked in medially) (Fig. 5G). The spared posterior hippocampal tissue first appeared in this slice, with the right side showing more hippocampal head than the left (Fig. 5G).

The eighth image (Fig. 5H) embodied the presumptive uncal hippocampus and anterior dentate gyrus level, where neighboring anatomical landmarks were the cerebral peduncles, red nucleus, substantia nigra in the brainstem, anterior nucleus of the thalamus and posterior putamen. In the ninth image (Fig. 5I), the right hippocampus began to resemble the classic hippocampal shape, and this slice showed the body of the hippocampus for the first time. The tenth image exposed the body of the hippocampus where the lateral geniculate nucleus of the thalamus made its first appearance, defining the end of the entorhinal cortex (Fig. 5J). Images ten and eleven revealed badly damaged parahippocampal gyri, especially on the left side (Figs. 5J,K). Images eleven and twelve showed the shrunken posterior body and tail of the hippocampus (Figs. 5K,L). In the twelfth image, the posterior thalamus (pulvinar), fimbria-fornix, and posterior commissure all came into view (Fig. 5L).

In summary, the high-resolution, high-contrast images reported here indicated that the areas removed bilaterally by suction during H.M.’s experimental operation were the medial temporopolar cortex, piriform cortex, virtually all of the entorhinal cortex, most of the perirhinal cortex (area 35), a large amount of subiculum, amygdala, except the dorsal most nuclei (i.e., central and medial), most of the hippocampus (head and body), and the dentate gyrus (posterior head and body). Parts of posterior parahippocampal gyrus (roughly equivalent to TH and TF) remained but were damaged. Other medial temporal lobe areas spared bilaterally were: the dorsal-most amygdala, part of the hippocampal-amygdalo-transition-area, a portion of perirhinal area 35, a medial portion of the hippocampus or gyrus ambiens, and the posterior body and tail of the hippocampus. The major sulci in the medial temporal lobe were remarkably well preserved bilaterally, with the exception of the hippocampal fissure. The collateral sulci were partially present, but shallow. The endorhinal sulci were present dorsally and medially, the sulci semi-annularis were spared medially, but the rhinal sulci were absent rostrally.

Ex Vivo MRI

At higher field strength (7.0 T), we acquired ultra-high-resolution images at 210 μm for the whole brain. Because the brain was suspended in 4% paraformaldehyde during scanning, the background contained some MRI signal from the water molecules in the solution. The contrast to noise ratio (CNR) and signal to noise ratio (SNR) were compromised for two reasons—the tissue contrast and solution contrast were similar, and the resolution was high. Due to the preciousness of this brain, we chose not to subject it to a proton-free liquid, such as Fomblin. Had we used a proton-free liquid, we would have avoided the unsatisfactory background observed in the 7.0 T images (Fig. 6). Even with the high background, however,

the ex vivo scans showed new details, and we delineated specific landmarks, such as the endorhinal sulcus and collateral sulcus, which helped determine the exact boundaries of the lesion. We outlined the lesion with dotted lines at three pertinent anterior-posterior levels: the anterior commissure, columns of fornix, and mammillary bodies. The high-resolution ex vivo scans provided additional information about the exact shape of H.M.'s lesions.

At the level of the anterior commissure, the anterior-most levels of the entorhinal cortex (i.e., the piriform cortex) and the extreme anterior parts of amygdala were removed (Fig. 6A). It is noteworthy that at this level, the lesion represented a rectangular shape and showed sharp 90° angles at the innermost (and superior) borders.

The second level is at the columns of the fornix (Fig. 6B). At this mid-amygdala level, the lesion shape, indicated by the dotted white lines, became irregular, especially on the left (Fig. 6B). The white arrow points to tissue that was likely the anterior hippocampus.

The third medial temporal lobe level is at the mammillary bodies of the hypothalamus, where the hippocampal head is largest. The right lesion appeared significantly larger than the left in the medial-lateral direction, consistent with our lesion measurements. Based on the quantitative data and these qualitative data, the right-sided lesion was slightly shorter than the left-sided in the anterior-posterior plane but slightly wider in the medial-lateral plane.

Lesion Size

We defined the overall length and width of H.M.'s lesion as the distance parallel to the anterior-posterior direction and left-right direction, respectively. We considered the lesion measurements in two ways, the total ablation and the total ablation plus damaged cortex. For the left-sided lesion, the length from the tip of the temporal lobe was 4.6 cm for the ablation and 6.0 cm for the ablation and damaged cortex (Fig. 7). For the right-sided lesion, the length from the tip of the temporal lobe was 4.2 cm for the ablation and 5.5 cm for the ablation and damaged cortex (Fig. 7). These dimensions indicated that the left medial temporal lobe lesion was larger than the right. The width was 2.04 cm on the left and 1.89 cm on the right at the temporal pole, 1.54 cm on the left and 1.63 cm on the right at the amygdala/uncus, and 1.02 cm on the left and 0.95 cm on the right at the hippocampal tail. The overall shape of the lesion matched a truncated cone with the wide base anterior and the narrow end posterior.

We also obtained two high-resolution anatomical volumes—the 440 μm in situ volume and the 210 μm ex vivo volume. Both were synthesized from multiple FLASH scans collected at different flip angles. The in situ 440 μm volume had near in vivo contrast, with gray matter appearing darker than white matter and CSF that was dark, but not black (visible also in the vicinity of the lesion).

The ex vivo 210 μm volume had a different contrast because the tissue was fixed (tissue classes are better distinguished by T2* contrast in fixed ex vivo brain tissue) (Tovi and Ericsson, 1992). In these images, gray matter was brighter than white matter and exhibited distinct layers, such as the *stria Gennari*, which were not visible in the in situ scans. Because

the brain was packed in paraformaldehyde, which generated a relatively strong signal that was comparable to white matter, the ventricles and region of the lesion were not extremely distinct from the adjacent structures. The cotton packing and the brain contained small bubbles, and the latter gave rise to spin dephasing artifacts, which were exaggerated by the choice of a long TE, a consequence of the low bandwidth needed to obtain reasonable SNR and gradient strengths at the required high resolution.

The white matter was noticeably inhomogeneous in both the in situ and ex vivo images, presumably a consequence of aging-related white matter disease. In the ex vivo images, $B1^+$ (RF transmit field) inhomogeneities due to the dielectric resonance effect at high field contributed further to overall image non-uniformity. Despite the fact that we invested 15.5 hrs in the 210 μm volumes vs. 2.5 hrs for the 440 μm, SNR was higher for the 440 μm volume because SNR falls dramatically with increasing isotropic resolution. SNR was roughly 20 to 50 and 130 to 150 for brain tissue in the 210 μm and 440 μm volumes, respectively. These values are approximate because SNR varies spatially, and the noise distribution is not precisely Gaussian. We selected protocols that would give reasonable SNR in the time available. The CNR (gray/white) for the 440 μm data was 14.7. In the 210 μm data, CNR measures for gray/white matter were 15.1 for high signal areas and 5.7 for medium signal areas. The SNR measures in these regions were 4.24 and 3.39, respectively (Fig. 4).

Structures Outside the Medial Temporal Lobes

Cerebellum—The cerebellum was severely atrophic and at autopsy appeared nearly half the size of a healthy cerebellum. The cerebellar atrophy seemed uniform with the flocculonodulus, vermis, and lateral hemispheres all reduced in size. In the in situ MRI images, we observed the dentate nucleus, the largest of the deep cerebellar nuclei, in its usual location, but we could not detect the other nuclei (fastigial, globose, emboliform), given the resolution $(440\ um)^3$.

Aging-related changes—At the end of his life, H.M. became demented. Multiple small strokes due to untreated hypertension and white matter atrophy likely contributed to his mental deterioration. The black spots in the MRI images indicate hypertensive disease and were particularly notable in the brainstem in Figure 4A. As a consequence of the untreated hypertension and perhaps other aging processes, we observed extensive isocortical and subcortical atrophy in all structures. Limbic structures such as the fornix, hippocampal commissure, and mammillary bodies, which were connected to the hippocampus before the surgery, were markedly degenerated (Fig. 5G). Similarly, the extended amygdala (centromedial amygdala and bed nucleus of stria terminalis) and other structures (i.e., the substantia inominata, including the nucleus basalis of Meynert and the diagonal band of Broca) showed noteworthy deterioration, as did the ventral striatopallidal areas. In the basal forebrain, the atrophy was so extensive that it was difficult to discern the location of nuclei. Degeneration went beyond the limbic cortices and limbic-related areas. We observed severe atrophy in the striatopallidum (caudate, putamen, globus pallidus) and thalamus (anterior nucleus, ventral anterior nucleus, mediodorsal nucleus, lateral posterior, lateral dorsal nucleus, pulvinar nucleus, medial geniculate nucleus and lateral geniculate nucleus) as

demonstrated by the large size of the third ventricle (Figs. 5H–J). We noted atrophy of the anterior commissure and all parts of the corpus callosum. The corpus callosum appeared so thin that it resembled the thickness of a healthy anterior commissure. We found isocortical thinning in all areas, including primary and secondary sensory and motor cortices. Shrinkage was especially pronounced in prefrontal, temporal, parietal, and occipital association areas.

White Matter Integrity

The diffusion imaging data acquired as part of the imaging sessions will be reported at a later time. The structural images, however, demonstrated a clear and substantial deterioration of the connective integrity of H.M.'s brain, with overt macrostructural white matter lesions throughout several portions of the cerebrum (Fig. 5). We previously described this damage and noted that hints of white matter deterioration were apparent as far back as 1998 when he was 72 (Corkin et al., 1997; Salat et al., 2006). In the 2008 imaging sessions, dark bands of hypointense white matter in T1 images were obvious throughout the periventricular regions. Such changes are commonly observed in older adults, but the degree of alterations here was well beyond what could be considered a benign consequence of aging.

Blood Supply

We did not explicitly trace the blood vessels in H.M.'s brain, but based on the anatomical areas that were surgically removed, it is likely that the blood supply was also interrupted. The arterial origins of the vascular supply to the medial temporal lobe include the middle cerebral artery, internal carotid artery, anterior choroidal artery, and posterior cerebral artery. From the fresh brain, it appeared that the anterior temporal artery, a branch of the posterior cerebral artery was removed bilaterally. The anterior choroidal artery, known to supply the anterior hippocampus, was absent on both sides, as was the anteroinferior parahippocampal artery, which supplies the anterior parahippocampal gyrus (i.e., entorhinal cortex). The posterior temporal artery was spared on both sides (Figs. 2 and 3) as well as the posterior parahippocampal artery, which supplies the posterior parahippocampal gyrus (i.e., TH and TF). Further tissue damage suggested that the posterior hippocampal artery, which supplies the posterior hippocampus, was compromised bilaterally.

DISCUSSION

The onset of H.M.'s profound memory impairment immediately after the operation established for the first time that removal of the hippocampus and surrounding structures causes amnesia (Scoville and Milner, 1957). The postmortem studies reported here are part of an ongoing effort to characterize the damage as precisely as possible. Our first goal was to document in detail the medial temporal lobe lesions, and the second was to examine the integrity of other structures that likely supported his intact intellect and preserved learning capacities. Bearing this anatomical information in mind, we associate specific cognitive processes that were impaired or spared in H.M. to particular circuits inside and outside the medial temporal lobe. Many of the findings with H.M. informed ongoing controversies in cognitive neuroscience concerning dissociations of function.

This report extends previous anatomical findings in MRI by revealing more detail and specific anatomy about what structures were removed or spared. The autopsy photographs showed the dense scar tissue in H.M.'s lesion and the marked cerebellar atrophy, while the MRI data, including in situ and ex vivo images, capitalized on improved contrast and resolution to reveal the lesion shape (or remaining tissue shape) and the precise measurements for lesion size. For example, the improved contrast highlighted tissue that may be the gyrus ambiens or a sliver of the anterior uncus. It is difficult to estimate whether this tissue is gyrus ambiens (medial part of entorhinal cortex) or uncal hippocampal tissue (i.e., medial CA1) and this new finding must be evaluated histologically. The high-resolution MRI also showed contrast differences between damaged and undamaged tissue that allowed more precise measurement of overall lesion size and shape. In this report, the lesion, measured from 440 μm^3 MRI, was 6.0 cm on the right and 5.5 cm on the left, suggesting that Scoville (Scoville and Milner, 1957) overestimated the lesion at 8 cm while Corkin and colleagues (Corkin et al., 1997) slightly underestimated the right-sided lesion at 5.1 cm. The high-resolution MRI also revealed the shape of the lesions, which exactly followed the contour of the parahippocampal gyrus, wider anteriorly and narrower posteriorly. Previous in vivo MRI images showed that H.M. developed significant white matter damage and cortical thinning as he aged (Salat et al., 2006). The new in situ MRI findings provide evidence of white matter disease progression, showing that at the time of H.M.'s death, his white matter was riddled with white matter signal abnormalities and extensive cortical thinning. Cortical thinning and white matter signal abnormalities were widespread, and no structure was spared. The following paragraphs review how H.M.'s lesions relate to the rich body of behavioral data collected over 55 years.

Lesion Dimensions

Overall lesion size—At the time of H.M.'s operation, Scoville estimated that the lesion extended 8 cm back from the tip of the temporal lobe. If this had been the case, then the damage would have invaded visual cortex, which it did not. With the advent of MRI, we were able to get a more accurate idea of lesion size. The in vivo MRI estimates in the rostrocaudal extent, based on 1 mm MRI data, were ~5.4 cm on the left and ~5.1 cm on the right (Corkin et al., 1997). The comparable postmortem MRI dimensions were slightly greater, showing that H.M.'s lesion was 6.0 cm on the left and 5.5 cm on the right (Fig. 7). The high-resolution in situ data allowed us to measure the excision and the damaged tissue more precisely. In the left temporal lobe, the excised region measured 4.6 cm, the damaged area an additional ~1.5 cm, and the entire lesion 6.0 cm. On the right side, the excision measured 4.2 cm, the damaged region an additional ~1.4 cm, and the whole lesion 5.5 cm. The ex vivo measures were more accurate because of the superior resolution we could obtain in long scan sessions at 3 T and 7 T that would not have been feasible in vivo. We hypothesize that the greater lesion size was due in part to age- and disease-related degeneration. The in situ MRI findings reported here are the most accurate measures of H.M.'s lesion size because the brain had not yet been distorted by removal and fixation procedures.

Correlation between lesion size, distribution, and severity of amnesia—H.M. had both extensive amnesia and large medial temporal lesions, suggesting that amnesia

severity is related to lesion size. His amnesia was more profound than that of Penfield and Milner's patients F.C. and P.B., whose excisions for epilepsy and pre-existing damage spared a considerable amount of medial temporal tissue (Penfield and Milner, 1958; Milner, 1959). More recent findings from Squire's laboratory extend the evidence concerning correlations with lesion size and support the view that lesions restricted to the hippocampus produce less severe memory loss than lesions of the hippocampus plus other temporal lobe areas. R.B.'s lesion, limited to the CA1 field, resulted in moderately severe amnesia (Zola-Morgan and Squire, 1986), whereas two other patients, G.P. and E.P., with damage to their entire medial temporal lobes bilaterally, were profoundly amnesic (Stefanacci et al., 2000; Bayley and Squire, 2005). Notably, E.P.'s lesion included the temporal pole, amygdala, entorhinal cortex, hippocampus, perirhinal cortex, and rostral parahippocampal cortex and also extended into lateral temporal neocortex; his declarative memory was even more impaired than H.M.'s (Insausti et al., 2013).

Medial Temporal Lobe Structures Excised and Spared

After H.M.'s death in 2008, we assessed his lesion using high-resolution in situ and ex vivo MRI. These images showed that the following areas were removed or damaged: substantial portions of the medial temporopolar, piriform, entorhinal, perirhinal, and parahippocampal cortices, as well as the subiculum, presubiculum, parasubiculum, amygdala, hippocampal fields CA1, CA2, CA3, and CA4 (in the hippocampal head and body), and dentate gyrus (posterior head and body). Further, our analyses suggested that a few noteworthy structures survived the medial temporal lobe surgery and may have been more difficult to discern with in vivo MRI scans due to lower resolution (Corkin et al., 1997; Salat et al., 2006). Notably, several areas within the amygdala were spared—parts of the amygdalar medial nucleus, cortical nucleus, cortical amygdaloid transition area, amygdala-striatal zone, endopiriform nucleus, and a portion of the central nucleus. Also visible were the hippocampal-amygdalo-transition-area (HATA), a small portion of the uncus, the tail of the hippocampus (~2 cm), a small part of the perirhinal cortex (Brodmann area 35), the entire ectorhinal cortex (Brodmann area 36), and ~2 cm of the posterior parahippocampal gyrus. Although the residual hippocampal, perirhinal, and parahippocampal tissue was first documented in the 1992 and 1993 MRI images (Corkin et al., 1997), the present findings further specify the locus and extent of the spared tissue.

Neural Substrate for H.M.'s Amnesia

Parahippocampal cortices and hippocampal formation—After his operation in 1953, H.M. could not consolidate and retrieve new facts and events, documenting for the first time that circuits within the medial temporal lobe are necessary for the establishment of long-term declarative memory (Scoville and Milner, 1957). Memory experiments carried out over the next five decades showed that H.M.'s deficits were severe and extensive, affecting the acquisition of verbal and nonverbal material presented via four sensory modalities (Milner, 1968; Corkin, 1984, 2002). He could not learn new episodic or semantic information (Gabrieli et al., 1988; O'Kane et al., 2004), highlighting the critical role of medial temporal lobe structures in all kinds of declarative memory. Further support for this brain-behavior correlation came from MRI studies carried out in the 1990s, which gave a more accurate picture of the specific structures that were excised and spared in H.M.'s brain.

The postmortem studies reported here provide new details of his lesions that could not be gleaned from the in vivo imaging studies.

By far the greatest territory removed on the day of surgery was the parahippocampal gyrus, in particular, the anterior parts of the perirhinal cortex and the entire entorhinal cortex. In a normal brain, the entorhinal cortex receives input from several secondary and tertiary association cortices and multimodal areas (in prefrontal cortex and superior temporal association cortex) and acts as the ultimate end station before extrinsic sensory afferents converge prior to entering the hippocampus (Van Hoesen, 1997; Van Hoesen et al., 1972). After this convergence on the entorhinal cortex, entorhinal layer II and superficial layer III then project to the hippocampus via the perforant pathway (Van Hoesen and Pandya, 1975).

Scoville's resection included the mesocortices of the anterior parahippocampal gyrus (entorhinal and perirhinal cortices (perirhinal area 35)) and also the hippocampal head and body. As a result, H.M.'s perforant pathway was destroyed at its origin and termination, thereby eliminating the entire circuitry necessary for long-term declarative memory. The remaining ~2 cm of hippocampal tissue was deafferented, and, therefore, not able to support long-term memory formation, storage, and retrieval. A preliminary histological study showed that the remaining hippocampal tissue contained substantial gliosis, which would further compromise the residual tissue (Annese et al., 2014).

H.M.'s pervasive memory impairment resulted from the removal of a significant portion of his hippocampi, including all CA subfields, the anterior dentate gyrus, anterior subiculum, anterior presubiculum, and prosubiculum. The hippocampal remnants included the hippocampal-amygdala-transition-area (HATA), the tail of the hippocampus, and a small portion of medial hippocampal tissue. Subsequent histological studies will clarify whether the small medial remnant is uncus or gyrus ambiens. Also spared were the posterior portions of the subiculum, dentate gyrus, and hippocampal body and tail. The posterior portion of the subiculum appeared to be intact, possibly leaving the subicular projections to the anterior, lateral dorsal, reuniens, and paraventricular nuclei of the thalamus untouched (Aggleton et al., 1986). It is clear, however, that this modest input, if it existed, was not sufficient to support normal memory function in H.M.

A new finding in the postmortem scans concerned the medial temporal stem. In 1997, we reported that the temporal stem was intact (Corkin et al., 1997), although Gaffan disagreed (Gaffan, 2001). In the current study, major advances in technology allowed us to examine the temporal stem with greater precision in the in situ and ex vivo images. We noted that this structure was markedly deteriorated in H.M. in situ and showed decreased contrast in MPRAGE (see Figs. 5C–E). It is unclear whether these lesions dated back to the surgical excision or were caused by degenerative disease late in life, but we favor the view that this damage was due to aging and white matter deterioration as noted in previous MRIs (Salat et al., 2006) and not to Scoville's original resection. The role of the temporal stem in amnesia has been somewhat controversial (Horel, 1978; Gaffan et al., 2001; Gaffan, 2001), but a study by Zola-Morgan, Squire, and Mishkin (Zola-Morgan et al., 1982) appeared to be irrefutable. They found that monkeys in whom the temporal stem white matter had been cut bilaterally were unimpaired on a delayed nonmatching-to-sample task, whereas animals with

bilateral lesions of the amygdala, hippocampus, and parahippocampal gyrus showed severe impairment. A later study by Gaffan et al. was consistent with this view (Gaffan et al., 2001). On a delayed matching-to-sample task, the performance of monkeys with transection of the anterior temporal stem alone did not differ significantly from their preoperative levels. It is, therefore, unlikely that H.M.'s temporal stem lesions contributed to his declarative memory impairment. Rather, his profound amnesia was caused by the excision of the parahippocampal cortices and hippocampal formation. H.M.'s performance on delayed-match-to-sample and delayed-nonmatch-to-sample tasks was comparable to that of control participants 6 months after learning (Freed et al., 1987; Freed and Corkin, 1988), suggesting that his partially intact perirhinal cortex may have been engaged to carry out these tasks.

Aging, Cortical Thinning, and White Matter Damage

Previous in vivo MRIs characterized H.M.'s cortical and white matter damage (Salat et al., 2006). At the time of his death, he was demented, and his entire brain was severely atrophied, with no structure escaping degeneration. As noted previously (Annese et al., 2014), we observed a small lesion in the left orbitofrontal region in the in situ and ex vivo MRI scans that was not described in Scoville's original report (Scoville and Milner, 1957). The etiology of this lesion is unclear, but we are confident that planned histological studies will reveal the cause. The possibilities include damage by the retractor used to elevate H.M.'s left frontal lobe, deafferentation of a medial temporal lobe projection, or white matter disease, possibly due to small vessel ischemic disease, such as untreated hypertension. The white matter damage throughout H.M.'s brain was severe in the in situ and ex vivo images, and it was far worse than in other untreated hypertensive cases at his age (JCA and DHS, personal observation) (Fazekas et al., 1993; Young et al., 2008). Substantial contrast changes in older adults may be due to significant dysfunction of vascular regulatory mechanisms (Braffman et al., 1988; Breteler et al., 1994b; Longstreth et al., 1996; Erkinjuntti, 2007), and given the substantial white matter abnormalities that we observed in H.M.'s brain ex vivo, it is likely that white matter damage caused his dementia.

Neural Substrates for H.M.'s Preserved Memory Capacities

H.M.'s deep and lasting amnesia attests to the fact that the spared medial temporal lobe structures were unable to support normal memory function or anything approaching it. Still, over the years, he occasionally surprised his examiners by retrieving episodic and semantic information that he encountered after his operation. The most astonishing example came from a picture recognition experiment in which we asked him to look at and remember complex colorful pictures for 20 sec each. Not only did he achieve normal recognition at 10 min, 24 hrs, 72 hrs, and 1 wk after encoding, but he also scored within 1 SD of the control mean 6 months later (Freed et al., 1987; Freed and Corkin, 1988).

We attribute H.M.'s ability to recognize the complex pictures to the engagement of familiarity–based processes supported by his residual perirhinal and parahippocampal cortices in communication with his preserved cortical circuitry. Our MRI data obtained in vivo and in situ showed some remnants of perirhinal and parahippocampal cortices bilaterally (Figs. 5E–G) (Corkin et al., 1997). Evidence accumulated over the last 20 years strongly suggests that recollection and familiarity engage different medial temporal lobe

areas, with recollection mediated by the hippocampus and familiarity by perirhinal and parahippocampal cortices (Aggleton and Brown, 1999, 2005; Yonelinas and Jacoby, 2012). H.M.'s ability to recognize complex visual stimuli underscores the point that the hippocampus is not necessary for recognition memory based on familiarity.

H.M. was also able to recognize and provide a few distinguishing details about celebrities and politicians who rose to fame after his operation, such as JFK, Ray Charles, and Liza Minnelli (Gabrieli et al., 1988; O'Kane et al., 2004). We attribute these glimmers of memory formation in part to processing in preserved medial temporal lobe structures seen in the in situ and ex vivo MRI images: part of perirhinal cortex, posterior parahippocampal cortex, dorsal-most amygdala, and the medial-most uncus. It is possible that these small pieces of medial temporal lobe that remained, especially posteriorly, helped support declarative memory formation on rare occasions. H.M. spent a lot of time watching television and leafing through magazines, which exposed him to a wealth of information about celebrities. This repeated stimulation over months and years enabled him to build up meager representations of a handful of famous people; he acquired this knowledge slowly over time and not via the fast declarative memory processes that healthy individuals would employ.

H.M.'s preserved memory capacities also included those now classified as nondeclarative. Milner's 1962 groundbreaking report that he showed procedural learning over three days introduced the idea that the human brain houses dissociable memory circuits (Milner, 1970). Subsequent experiments extended this result, showing that H.M. could acquire a variety of motor skills (Corkin, 1968). Studies in patients with Parkinson disease, Huntington disease, and cerebellar degeneration later indicated that the striatum and cerebellum mediate motor skill learning (Sanes et al., 1990; Knopman and Nissen, 1991; Pascual-Leone et al., 1993; Breteler et al., 1994a,b; Corkin, 2013). Our in vivo MRI results confirmed that the striatum was not damaged in H.M.'s operation, and although his cerebellum was atrophied, it did not appear grossly abnormal.

Subsequent studies evaluated H.M.'s performance on other kinds of nondeclarative memory tasks. In a series of eyeblink classical conditioning experiments, he acquired conditioned responses in both the delay and trace paradigms (Woodruff-Pak, 1993). Although he required more trials to reach criterion than his control, the fact that he showed any conditioned responses is a challenge to explain because previous research has established that the cerebellum, hippocampus, and amygdala play a major role in eyeblink conditioning (Woodruff-Pak et al., 1985; Weisz et al., 1992; Thompson and Kim, 1996; Clark et al., 2002; Christian and Thompson, 2003; Thompson and Steinmetz, 2009). In H.M.'s brain, the hippocampus and amygdala were extirpated, and the cerebellum was markedly atrophied. Still, it is possible that his cerebellum and deep cerebellar nuclei supported the learning, and we will examine these structures microscopically in hope of uncovering clues about his ability to acquire conditioned responses.

Repetition priming refers to a kind of learning in which recent incidental exposure to test stimuli, such as words, pictures, and patterns, facilitates subsequent processing of that information. Priming is evidence that past experience can influence memory unconsciously, that is, when participants are not trying intentionally to recall the past, and it is mediated by

cortical pathways undamaged in H.M. In several experiments, he demonstrated intact performance on perceptual and conceptual priming tasks (Gabrieli et al., 1990, 1995; Keane et al., 1995). Companion studies in patients with cortical lesions indicated that conceptual priming is mediated by lateral temporal and parietal circuits, while perceptual priming depends on occipital circuits (Keane et al., 1991, 1994, 1995; Gabrieli et al., 1994). These cortical networks were intact in H.M. and likely the underpinnings of his intact priming performance. This finding of preserved nondeclarative memory considered side by side with his impoverished declarative memory, measured by tests of recall and recognition, established the validity of cognitive and neural dissociations among memory processes.

Neural Substrates for H.M.'s Nonmnemonic Behavioral Deficits

Examination of H.M.'s fresh brain at autopsy indicated that his olfactory bulbs and tract were undamaged, but the surgical removal did include primary olfactory cortex in the temporal lobe (piriform cortex and periamygdaloid cortex). As a result, H.M. was anosmic. Extensive behavioral testing uncovered limited preserved function and severe deficits on several olfactory tasks (Eichenbaum et al., 1983). His detection of weak odorants was normal as was his threshold for discrimination of intensity differences, and he showed normal adaptation to a strong odor. In contrast, his ability to discriminate odor quality was completely absent on three different measures: signal-detection testing, the triangle match-to-sample task, and a common-odor-matching task, likely due to the absence of piriform and periamygdaloid cortices (Eichenbaum et al., 1983). This striking dissociation of olfactory perceptual capacities established that odor quality discrimination and recognition are not necessary for detection, intensity discrimination, or adaptation.

The in situ and ex vivo MRI studies described here brought to light the details of H.M.'s extensive amygdala resection, which included the lateral, basolateral, accessory basal, and paralaminar nuclei, a portion or all of the central nucleus, and the anterior amygdala area. The result was that most of H.M.'s amygdala output was silenced, and it is likely that the amygdala resection explains a cluster of behavioral abnormalities. H.M.'s perception of pain was diminished in the laboratory and in daily life, he showed no change in his ratings of hunger and thirst from before to after a meal, he was asexual, and he was not fearful of anything (Hebben et al., 1985; Corkin, 2013). Nevertheless, he could experience and display a range of emotions, such as happiness, friendliness, sadness, worry, guilt, and aggression, and he was able to label the emotion in various facial expressions (Corkin, 2013). The emotional response system is complex, and the underlying brain mechanisms connecting inputs and outputs engage cortical and subcortical circuits beyond the amygdala (Price, 2003). A goal of future histological studies will be to examine the integrity of these connections and remnants of the amygdala in H.M.'s brain.

Neural Substrate for H.M.'s Preserved Cognitive Capacities

The MR images collected from H.M. in 1992 and 1993, four decades after his operation, showed that his frontal, parietal, and occipital cortices were normal for his age, as was the lateral temporal neocortex. At that time, it was unclear whether the subcortical white matter associated with the most anterior portions of the superior, middle, and inferior temporal gyri was damaged, but our in situ and ex vivo images confirmed that these tracts were abnormal.

Nevertheless, the vast expanse of cortex on both sides of H.M.'s brain likely functioned near optimally, allowing the engagement of multiple specialized circuits to support his performance on a broad spectrum of cognitive tasks.

Milner conducted H.M.'s first postoperative psychological examination in 1955, 2 years after his operation (Scoville and Milner, 1957). On the Wechsler-Bellevue Intelligence Scale, he achieved an IQ of 112, but on the Wechsler Memory Scale, his MQ was only 67, indicating normal intelligence coupled with markedly impaired long-term memory (Wechsler, 1945). On subsequent testing with different forms of the Intelligence Scale and Memory Scale, he maintained this pattern of performance through 2000 (Kensinger et al., 2001). This longitudinal analysis firmly established that medial temporal lobe structures are not necessary for optimal performance on IQ tests, indicating a clear dissociation between high-order cognition and long-term declarative memory.

The high-resolution, high-contrast MRI methods highlighted here confirmed that H.M.'s cortical and subcortical language areas remained intact following his surgery, and the results from numerous experimental measures and standardized tests showed that his language functions were largely spared (Kensinger et al., 2001). He successfully completed seven lexical memory tasks: spelling; picture naming, name recognition, and information retrieval; Boston naming test; picture naming; picture judgment; category identification; and landmark identification, and on tests of morphology, he was able to produce and judge regular and irregular inflectional or derivational forms, including plural production, past-tense production, past tense judgment, and derivational morphology production. Two additional tasks measured his syntax processing, and he performed them normally. In general, H.M. maintained his preoperative lexical knowledge without explicit retraining, indicating that medial temporal lobe structures are not necessary for the retention of already learned lexical information. They are, however, critical for the acquisition of new lexical information (e.g., new vocabulary, celebrities) (Gabrieli et al., 1988; Postle and Corkin, 1998). Notable exceptions in the language domain were H.M.'s impaired performance on fluency tasks and uneven success in detecting linguistic ambiguities (Lackner, 1974; Corkin, 2013). These deficits likely stemmed from a combination of factors: minimal surgical damage to anterolateral temporal cortex, slow responding, substandard education, and lower socioeconomic background (Kensinger et al., 2001; Schmolck et al., 2002).

Evidence of preserved problem solving and working memory processes came from H.M.'s consistently excellent performance on the Wisconsin Card Sorting Test (Milner, 1968). During each administration of the task over years of testing, he quickly changed to a new sorting category as needed and had very few perseverative errors, but he was always unaware that he had done the test before. To perform this complex task, H.M. had to recruit multiple cognitive processes and engage circuits in prefrontal cortex and posterior parietal cortex, areas that were spared in the 1953 surgery (Corkin et al., 1997; Salat et al., 2006).

H.M.'s bilateral medial temporal lobe resection was circumscribed, and the resulting amnesia was pure. He revolutionized the science of memory through his participation in numerous behavioral and imaging studies, and he continues to illuminate the science of memory. During his lifetime, neuroimaging advanced with specialized sequences and

sophisticated multichannel array coils that enabled high resolution MRI. These tools allowed a final and riveting inspection of H.M.'s lesions and remaining anatomy. This postmortem research is consistent with his wishes: He knew he was contributing to science and gladly donated his brain for future study. His mantra was, "Whatever is beneficial." It is fitting that the field of neuroscience continues to benefit from his contributions, even after his death.

Acknowledgments

The authors are grateful to H.M. and his conservator for the generous tissue donation. The authors also thank M. Dylan Tisdall, Jonathan R. Polimeni, and Thomas Witzel for technical assistance in developing protocols to accommodate extremely large data files and Kristen Huber for photographing the blockface images and laboratory preparations.

Grant sponsor: National Center for Research Resources; Grant number: P41-RR14075; Grant sponsor: NCRR BIRN Morphometric Project; Grant numbers: BIRN002 and U24 RR021382; Grant sponsor: National Institute for Biomedical Imaging and Bioengineering; Grant number: R01EB006758; Grant sponsor: National Institute on Aging; Grant numbers: AG022381 and 5R01AG008122-22; Grant sponsor: NIH Blueprint for Neuroscience Research; Grant number: 5U01-MH093765; Grant sponsors: Part of the Multi-Institutional Human Connectome Project and National Science Foundation; Grant number: NSF-SGER0714660; Grant sponsor: Dana Foundation; Grant number: 2007-4234.

References

Aggleton JP, Brown MW. Episodic memory, amnesia, and the hippocampal-anterior thalamic axis. Behav Brain Sci. 1999; 22:425–444. discussion 444–489. [PubMed: 11301518]

Aggleton JP, Brown MW. Contrasting hippocampal and perirhinal cortex function using immediate early gene imaging. Q J Exp Psychol B. 2005; 58:218–233. [PubMed: 16194966]

Aggleton JP, Desimone R, Mishkin M. The origin, course, and termination of the hippocampothalamic projections in the macaque. J Comp Neurol. 1986; 243:409–421. [PubMed: 3512627]

Annese J, Schenker-Ahmed NM, Bartsch H, Maechler P, Sheh C, Thomas N, Kayano J, Ghatan A, Bresler N, Frosch MP, Klaming R, Corkin S. Postmortem examination of patient H.M.'s brain based on histological sectioning and digital 3D reconstruction. Nat Commun. 2014; 5:3122. [PubMed: 24473151]

Bayley PJ, Squire LR. Failure to acquire new semantic knowledge in patients with large medial temporal lobe lesions. Hippocampus. 2005; 15:273–280. [PubMed: 15523609]

Benner T, Wisco JJ, van der Kouwe AJ, Fischl B, Vangel MG, Hochberg FH, Sorensen AG. Comparison of manual and automatic section positioning of brain MR images. Radiology. 2006; 239:246–254. [PubMed: 16507753]

Braak H, Braak E. On areas of transition between entorhinal allocortex and temporal isocortex in the human brain. Normal morphology and lamina-specific pathology in Alzheimer's disease. Acta Neuropathol. 1985; 68:325–332. [PubMed: 4090943]

Braffman BH, Zimmerman RA, Trojanowski JQ, Gonatas NK, Hickey WF, Schlaepfer WW. Brain MR: Pathologic correlation with gross and histopathology. 2. Hyperintense white-matter foci in the elderly. AJR Am J Roentgenol. 1988; 151:559–566. [PubMed: 3261518]

Breteler MM, van Amerongen NM, van Swieten JC, Claus JJ, Grobbee DE, van Gijn J, Hofman A, van Harskamp F. Cognitive correlates of ventricular enlargement and cerebral white matter lesions on magnetic resonance imaging. The Rotterdam Study. Stroke. 1994a; 25:1109–1115. [PubMed: 8202966]

Breteler MM, van Swieten JC, Bots ML, Grobbee DE, Claus JJ, van den Hout JH, van Harskamp F, Tanghe HL, de Jong PT, van Gijn J, et al. Cerebral white matter lesions, vascular risk factors, and cognitive function in a population-based study: The Rotterdam Study. Neurology. 1994b; 44:1246–1252. [PubMed: 8035924]

Brodmann, K. English translation by Laurence Garey of the German book, translator. London, UK: Smith-Gordon; 1909. Brodmann's 'Localisation in the Cerebral Cortex.

Clark RE, Manns JR, Squire LR. Classical conditioning, awareness, and brain systems. Trends Cogn Sci. 2002; 6:524–531. [PubMed: 12475713]

Corkin S. Acquisition of motor skill after bilateral medial temporal lobe excision. Neuropsychologia. 1968; 6:255–265.

Corkin S. Lasting consequences of bilateral medial temporal lobectomy: Clinical course and experimental findings in H.M. Semin Neurol. 1984; 4:249–259.

Corkin S. What's new with the amnesic patient H.M.? Nat Rev Neurosci. 2002; 3:153–160. [PubMed: 11836523]

Corkin, S. Permanent Present Tense: The Unforgettable Life of the Amnesic Patient, H. M. New York: Basic Books; 2013. p. 400

Corkin S, Amaral DG, Gonzalez RG, Johnson KA, Hyman BT. H. M.'s medial temporal lobe lesion: Findings from magnetic resonance imaging. J Neurosci. 1997; 17:3964–3979. [PubMed: 9133414]

Dale AM, Fischl B, Sereno MI. Cortical surface-based analysis. I. Segmentation and surface reconstruction. Neuroimage. 1999; 9:179–194. [PubMed: 9931268]

Deoni SC. High-resolution T1 mapping of the brain at 3T with driven equilibrium single pulse observation of T1 with high-speed incorporation of RF field inhomogeneities (DESPOT1-HIFI). J Magn Reson Imaging. 2007; 26:1106–1111. [PubMed: 17896356]

Deoni SC, Peters TM, Rutt BK. High-resolution T1 and T2 mapping of the brain in a clinically acceptable time with DESPOT1 and DESPOT2. Magn Reson Med. 2005; 53:237–241. [PubMed: 15690526]

Deoni SC, Rutt BK, Peters TM. Rapid combined T1 and T2 mapping using gradient recalled acquisition in the steady state. Magn Reson Med. 2003; 49:515–526. [PubMed: 12594755]

Ding SL, Van Hoesen GW. Borders, extent, and topography of human perirhinal cortex as revealed using multiple modern neuroanatomical and pathological markers. Hum Brain Mapp. 2010; 31:1359–1379. [PubMed: 20082329]

Ding SL, Van Hoesen GW, Cassell MD, Poremba A. Parcellation of human temporal polar cortex: A combined analysis of multiple cytoarchitectonic, chemoarchitectonic, and pathological markers. J Comp Neurol. 2009; 514:595–623. [PubMed: 19363802]

Eichenbaum H, Morton TH, Potter H, Corkin S. Selective olfactory deficits in case H.M. Brain. 1983; 106:459–472. [PubMed: 6850278]

Erkinjuntti T. Vascular cognitive deterioration and stroke. Cerebrovasc Dis. 2007; 24(Suppl 1):189–194. [PubMed: 17971655]

Fazekas F, Kleinert R, Offenbacher H, Schmidt R, Kleinert G, Payer F, Radner H, Lechner H. Pathologic correlates of incidental MRI white matter signal hyperintensities. Neurology. 1993; 43:1683–1689. [PubMed: 8414012]

Fischl B, Salat DH, Busa E, Albert M, Dieterich M, Haselgrove C, van der Kouwe A, Killiany R, Kennedy D, Klaveness S, et al. Whole brain segmentation: Automated labeling of neuroanatomical structures in the human brain. Neuron. 2002; 33:341–355. [PubMed: 11832223]

Fischl B, Salat DH, van der Kouwe AJ, Makris N, Segonne F, Quinn BT, Dale AM. Sequence-independent segmentation of magnetic resonance images. Neuroimage. 2004; 23(Suppl 1):S69–S84. [PubMed: 15501102]

Freed DM, Corkin S. Rate of forgetting in H.M.: 6-month recognition. Behav Neurosci. 1988; 102:823–827. [PubMed: 3214531]

Freed DM, Corkin S, Cohen NJ. Forgetting in H.M.: A second look. Neuropsychologia. 1987; 25:461–471. [PubMed: 3683805]

Gabrieli JD, Cohen NJ, Corkin S. The impaired learning of semantic knowledge following bilateral medial temporal-lobe resection. Brain Cogn. 1988; 7:157–177. [PubMed: 3377896]

Gabrieli JD, Milberg W, Keane MM, Corkin S. Intact priming of patterns despite impaired memory. Neuropsychologia. 1990; 28:417–427. [PubMed: 2377287]

Gabrieli JD, Keane MM, Stanger BZ, Kjelgaard MM, Corkin S, Growdon JH. Dissociations among structural-perceptual, lexical-semantic, and event-fact memory systems in Alzheimer, amnesic, and normal subjects. Cortex. 1994; 30:75–103. [PubMed: 8004991]

Gabrieli JD, McGlinchey-Berroth R, Carrillo MC, Gluck MA, Cermak LS, Disterhoft JF. Intact delay-eyeblink classical conditioning in amnesia. Behav Neurosci. 1995; 109:819–827. [PubMed: 8554707]

Gaffan D. What is a memory system? Horel's critique revisited. Behav Brain Res. 2001; 127:5–11. [PubMed: 11718881]

Gaffan D, Parker A, Easton A. Dense amnesia in the monkey after transection of fornix, amygdala and anterior temporal stem. Neuropsychologia. 2001; 39:51–70. [PubMed: 11115655]

Gloor, P. The Temporal Lobe. Oxford University Press; New York and Oxford: 1995. p. 1997

Hebb, DO. The organization of behavior. New York, NY: Wiley; 1949.

Hebben N, Corkin S, Eichenbaum H, Shedlack K. Diminished ability to interpret and report internal states after bilateral medial temporal resection: Case H.M. Behav Neurosci. 1985; 99:1031–1039. [PubMed: 3843537]

Horel JA. The neuroanatomy of amnesia. A critique of the hippocampal memory hypothesis. Brain. 1978; 101:403–445. [PubMed: 101278]

Insausti R, Tunon T, Sobreviela T, Insausti AM, Gonzalo LM. The human entorhinal cortex: A cytoarchitectonic analysis. J Comp Neurol. 1995; 355:171–198. [PubMed: 7541808]

Insausti R, Juottonen K, Soininen H, Insausti AM, Partanen K, Vainio P, Laakso MP, Pitkanen A. MR volumetric analysis of the human entorhinal, perirhinal, and temporopolar cortices. AJNR Am J Neuroradiol. 1998; 19:659–671. [PubMed: 9576651]

Insausti R, Annese J, Amaral DG, Squire LR. Human amnesia and the medial temporal lobe illuminated by neuropsychological and neurohistological findings for patient E.P. Proc Natl Acad Sci USA. 2013; 110:E1953–E1962. [PubMed: 23620517]

James, W. The Principles of Psychology: Dover Publications. New York: 1890. p. 1950

Keane MM, Gabrieli JD, Fennema AC, Growdon JH, Corkin S. Evidence for a dissociation between perceptual and conceptual priming in Alzheimer's disease. Behav Neurosci. 1991; 105:326–342. [PubMed: 2043276]

Keane MM, Gabrieli JD, Growdon JH, Corkin S. Priming in perceptual identification of pseudowords is normal in Alzheimer's disease. Neuropsychologia. 1994; 32:343–356. [PubMed: 8202228]

Keane MM, Gabrieli JD, Mapstone HC, Johnson KA, Corkin S. Double dissociation of memory capacities after bilateral occipital-lobe or medial temporal-lobe lesions. Brain. 1995; 118:1129–1148. [PubMed: 7496775]

Kensinger EA, Ullman MT, Corkin S. Bilateral medial temporal lobe damage does not affect lexical or grammatical processing: Evidence from amnesic patient H.M. Hippocampus. 2001; 11:347–360. [PubMed: 11530839]

Knopman D, Nissen MJ. Procedural learning is impaired in Huntington's disease: Evidence from the serial reaction time task. Neuropsychologia. 1991; 29:245–254. [PubMed: 1829141]

Lackner JR. Observations on the speech processing capabilities of an amnesic patient: Several aspects of H.M.'s language function. Neuropsychologia. 1974; 12:199–207. [PubMed: 4842381]

Longstreth WT Jr, Manolio TA, Arnold A, Burke GL, Bryan N, Jungreis CA, Enright PL, O'Leary D, Fried L. Clinical correlates of white matter findings on cranial magnetic resonance imaging of 3301 elderly people. The Cardiovascular Health Study. Stroke. 1996; 27:1274–1282. [PubMed: 8711786]

Lorente de No R. Studies on the structure of the cerebral cortex II Continuation of the study of ammonic system. J Fur Psychol Neurol. 1934; 46:113–177.

Milner B. The memory defect in bilateral hippocampal lesions. Psychiatr Res Rep Am Psychiatr Assoc. 1959; 11:43–58. [PubMed: 14422670]

Milner, B. Les troubles de la memorie accompagnant des lesions hippocampiques bilaterales. In: Passouant, P., editor. Physiologie de l'hippocampe. Paris: Centre National de la Recherche Scientifique; 1962. p. 257-272.

Milner, B. Biology of Memory. New York: Academic Press, Inc; 1970. Memory and the medial temporal regions of the brain; p. 29-50.

Milner B, Corkin S, Teuber H-L. Further analysis of the hippocampal amnesic syndrome: 14-year follow-up study of H.M. Neuropsychologia. 1968; 6:215–234.

Mugler JP III, Brookeman JR. Three-dimensional magnetization-prepared rapid gradient-echo imaging (3D MP RAGE). Magn Reson Med. 1990; 15:152–157. [PubMed: 2374495]

Mugler JP III, Bao S, Mulkern RV, Guttmann CR, Robertson RL, Jolesz FA, Brookeman JR. Optimized single-slab three-dimensional spin-echo MR imaging of the brain. Radiology. 2000; 216:891–899. [PubMed: 10966728]

O'Kane G, Kensinger EA, Corkin S. Evidence for semantic learning in profound amnesia: An investigation with patient H.M. Hippocampus. 2004; 14:417–425. [PubMed: 15224979]

Pascual-Leone A, Grafman J, Clark K, Stewart M, Massaquoi S, Lou JS, Hallett M. Procedural learning in Parkinson's disease and cerebellar degeneration. Ann Neurol. 1993; 34:594–602. [PubMed: 8215247]

Penfield W, Milner B. Memory deficit produced by bilateral lesions in the hippocampal zone. AMA Arch Neurol Psychiatry. 1958; 79:475–497. [PubMed: 13519951]

Postle BR, Corkin S. Impaired word-stem completion priming but intact perceptual identification priming with novel words: Evidence from the amnesic patient H.M. Neuropsychologia. 1998; 36:421–440. [PubMed: 9699950]

Price JL. Comparative aspects of amygdala connectivity. Ann N Y Acad Sci. 2003; 985:50–58. [PubMed: 12724147]

Roemer PB, Edelstein WA, Hayes CE, Souza SP, Mueller OM. The NMR phased array. Magn Reson Med. 1990; 16:192–225. [PubMed: 2266841]

Rosene, DL., Van Hoesen, GW. The hippocampal formation of the primate brain, a review of some comparative aspects of cytoarchitecture and connections. In: Jones, EG., Peters, A., editors. Cerebral Cortex. Further Aspects of Cortical Function, Including Hippocampus. New York: Plenum Press; 1987. p. 345-456.

Salat DH, Buckner RL, Snyder AZ, Greve DN, Desikan RS, Busa E, Morris JC, Dale AM, Fischl B. Thinning of the cerebral cortex in aging. Cereb Cortex. 2004; 14:721–730. [PubMed: 15054051]

Salat DH, van der Kouwe AJ, Tuch DS, Quinn BT, Fischl B, Dale AM, Corkin S. Neuroimaging H.M.: A 10-year follow-up examination. Hippocampus. 2006; 16:936–945. [PubMed: 17016801]

Sanes JN, Dimitrov B, Hallett M. Motor learning in patients with cerebellar dysfunction. Brain. 1990; 113:103–120. [PubMed: 2302528]

Schmolck H, Kensinger EA, Corkin S, Squire LR. Semantic knowledge in patient H.M. other patients with bilateral medial and lateral temporal lobe lesions. Hippocampus. 2002; 12:520–533. [PubMed: 12201637]

Scoville WB. The Limbic Lobe in Man. J Neurosurg. 1954; 11:64–66. [PubMed: 13131095]

Scoville WB, Milner B. Loss of recent memory after bilateral hippocampal lesions. J Neurol Neurosurg Psychiatry. 1957; 20:11–21. [PubMed: 13406589]

Stefanacci L, Buffalo EA, Schmolck H, Squire LR. Profound amnesia after damage to the medial temporal lobe: A neuroanatomical and neuropsychological profile of patient E. P. J Neurosci. 2000; 20:7024–7036. [PubMed: 10995848]

Steinvorth S, Levine B, Corkin S. Medial temporal lobe structures are needed to re-experience remote autobiographical memories: Evidence from H.M. and W.R. Neuropsychologia. 2005; 43:479–496. [PubMed: 15716139]

Thompson RF, Kim JJ. Memory systems in the brain and localization of a memory. Proc Natl Acad Sci USA. 1996; 93:13438–13444. [PubMed: 8942954]

Tovi M, Ericsson A. Measurements of T1 and T2 over time in formalin-fixed human whole-brain specimens. Acta Radiol. 1992; 33:400–404. [PubMed: 1389643]

Van der Kouwe, A., Benner, T. Combined brain morphometry and skull imaging with FLUSTER. Sydney; Australia: 2008.

van der Kouwe AJ, Benner T, Fischl B, Schmitt F, Salat DH, Harder M, Sorensen AG, Dale AM. On-line automatic slice positioning for brain MR imaging. Neuroimage. 2005; 27:222–230. [PubMed: 15886023]

van der Kouwe AJ, Benner T, Dale AM. Real-time rigid body motion correction and shimming using cloverleaf navigators. Magn Reson Med. 2006; 56:1019–1032. [PubMed: 17029223]

van der Kouwe AJ, Benner T, Salat DH, Fischl B. Brain morphometry with multiecho MPRAGE. Neuroimage. 2008; 40:559–569. [PubMed: 18242102]

Van Hoesen GW. Anatomy of the medial temporal lobe. Magnet Reson Imaging. 1995; 13:1047–1055.

Van Hoesen, GW. Cortical feedforward and cortical feedback neural systems in Alzheimer's disease. In: Hyman, BT.Duychaerts, C., Christen, Y., editors. Connections, Cognition and Alzheimer's Disease. Berlin, Heidelberg: Springer-Verlag; 1997.

Van Hoesen GW, Pandya DN. Some connections of the entorhinal (area 28) and perirhinal (area 35) cortices of the rhesus monkey. III. Efferent connections. Brain Res. 1975; 95:39–59. [PubMed: 1156868]

Van Hoesen GW, Pandya DN, Butters N. Cortical afferents to the entorhinal cortex of the Rhesus monkey. Science. 1972; 175:1471–1473. [PubMed: 4622430]

Van Hoesen, GW., Augustinack, JC., Dierking, J., Redman, SJ., Thangavel, R. The parahippocampal gyrus in Alzheimer's disease. Clinical and preclinical neuroanatomical correlates. In: Scharfman, W., Schwarcz, editors. The Parahippocampal Region, Implications for Neurological and Psychiatric Diseases. Ann N Y Acad Sci. Vol. 911. 2000. p. 254-274.

von Bonin, G., Bailey, P. The Neocortex of Macaca Mulatta. Urbana, IL: University of Illinois Press; 1947.

von Economo, C., Koskinas, GN. Atlas of Cytoarchitectonics of the Adult Human Cerebral Cortex. Karger Publications; Berlin: 1925.

Wechsler D. A standardized memory scale for clinical use. J Psychol. 1945; 19:87–95.

Weisz DJ, Harden DG, Xiang Z. Effects of amygdala lesions on reflex facilitation and conditioned response acquisition during nictitating membrane response conditioning in rabbit. Behav Neurosci. 1992; 106:262–273. [PubMed: 1317182]

Wiggins GC, Triantafyllou C, Potthast A, Reykowski A, Nittka M, Wald LL. 32-channel 3 T receive-only phased-array head coil with soccer-ball element geometry. Magn Reson Med. 2006; 56:216–223. [PubMed: 16767762]

Woodruff-Pak DS. Eyeblink classical conditioning in H.M.: Delay and trace paradigms. Behav Neurosci. 1993; 107:911–925. [PubMed: 8136067]

Yarnykh VL. Actual flip-angle imaging in the pulsed steady state: A method for rapid three-dimensional mapping of the transmitted radiofrequency field. Magn Reson Med. 2007; 57:192–200. [PubMed: 17191242]

Yonelinas AP, Jacoby LL. The process-dissociation approach two decades later: Convergence, boundary conditions, and new directions. Mem Cognit. 2012; 40:663–680.

Young VG, Halliday GM, Kril JJ. Neuropathologic correlates of white matter hyperintensities. Neurology. 2008; 71:804–811. [PubMed: 18685136]

Zola-Morgan S, Squire LR. Memory impairment in monkeys following lesions limited to the hippocampus. Behav Neurosci. 1986; 100:155–160. [PubMed: 3964416]

Zola-Morgan S, Squire LR, Mishkin M. The neuroanatomy of amnesia: Amygdala-hippocampus versus temporal stem. Science. 1982; 218:1337–1339. [PubMed: 6890713]

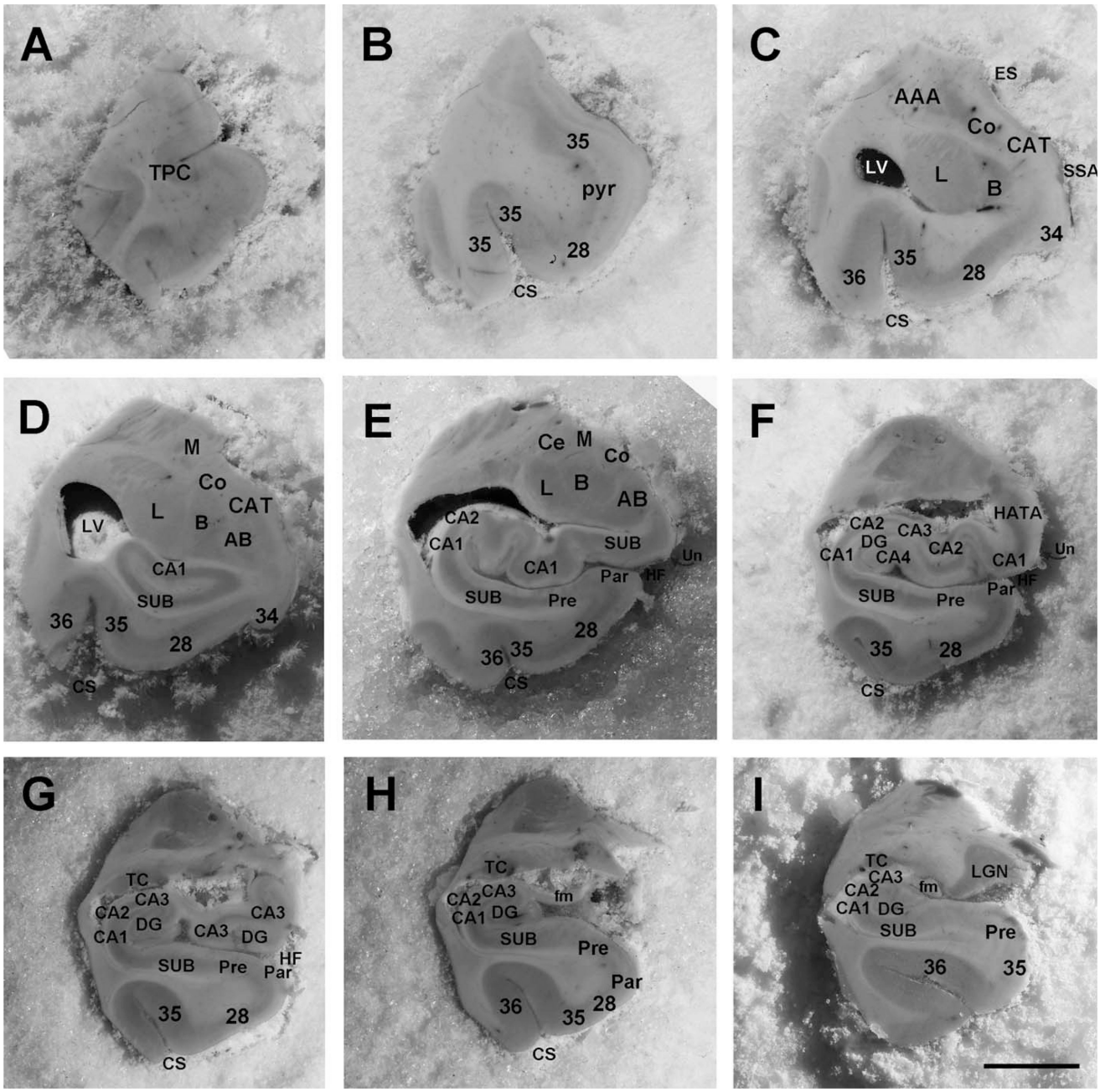

FIGURE 1.

Blockface images of medial temporal lobe structures from a control case (60-year-old, male). Nine levels represent the anterior-posterior extent of the medial temporal lobe. Level (A) temporal pole, (B) pyriform (olfactory) cortex, anterior-most entorhinal cortex, (C) anterior amygdala, (D) mid-amygdala, (E) anterior hippocampal head (pes), (F) posterior hippocampal head, (G) posterior hippocampal head and anterior hippocampal body, (H) hippocampal body, (I) posterior hippocampal body, hippocampal tail (not illustrated). Numerical labels correspond to Brodmann areas, and letter abbreviations are defined as: AAA = anterior amygdala area, AB = accessory basal nucleus of amygdala, B = basal nucleus of amygdala, CA = cornu ammonis (1–4), CAT = cortical amygdala transition area,

Ce = central nucleus of amygdala, Co = cortical nucleus of amygdala, CS = collateral sulcus, DG = dentate gyrus, ES = endorhinal sulcus, fm = fimbria, HATA = hippocampal amygdala transition area, HF = hippocampal fissure, L = lateral nucleus of amygdala, LV = lateral ventricle, M = medial nucleus of amygdala, Pre = presubiculum, Par = parasubiculum, SUB = subiculum, TP = temporal pole, and Un = uncus. Magnification bar = 1 cm.

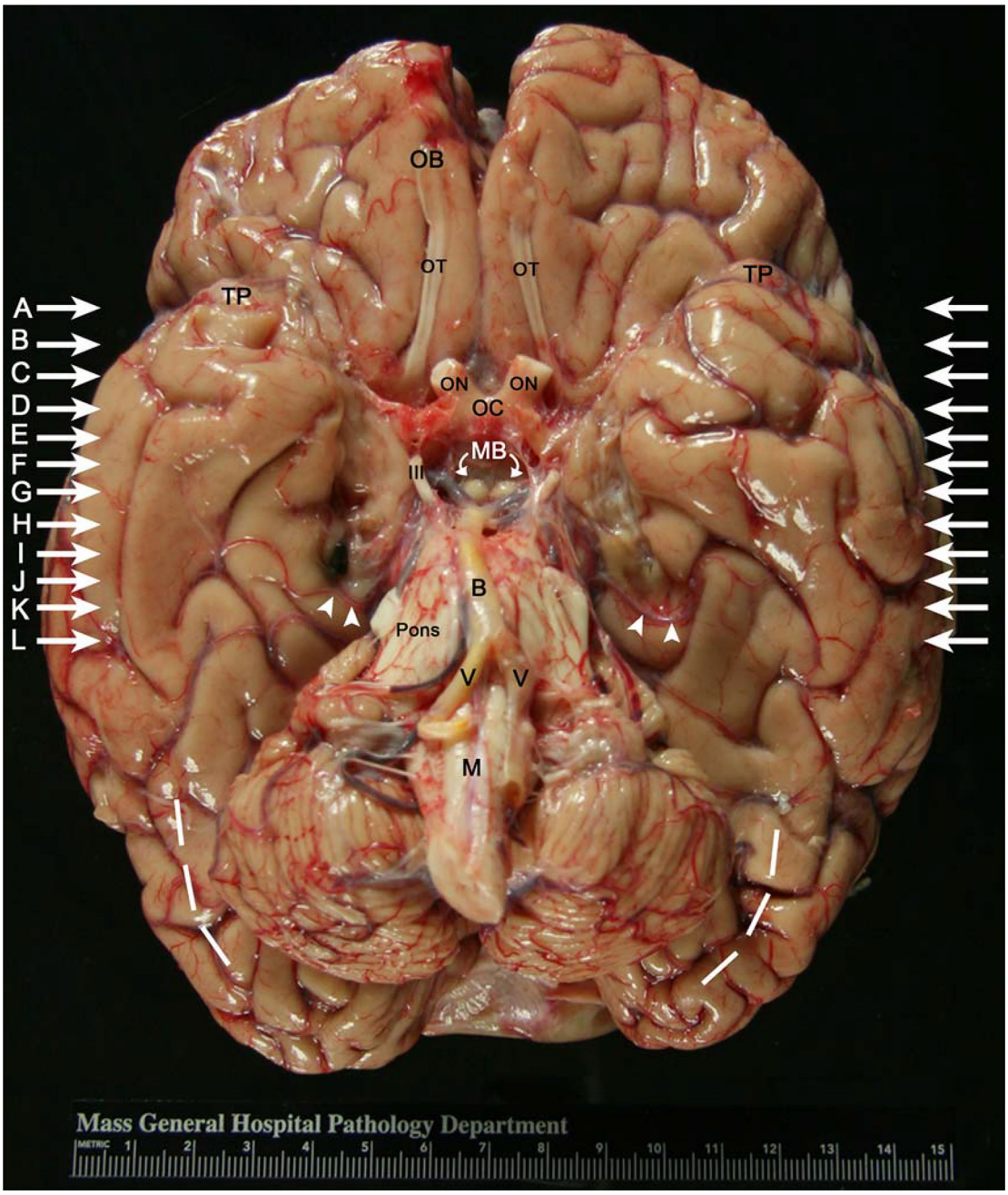

FIGURE 2.

Photograph of the whole fresh brain (inferior surface) taken at H.M.'s autopsy. In the ventral view, the white arrows on both sides of the brain indicate the lines of cut in the coronal MRI slices in Figure 5. These slices (white arrows) correspond to the in situ MRI (Figs. 5A–L). Note the area of excision and additional fibrous tissue (i.e., scar tissue) bilaterally, and the residual medial most tissue (bilaterally but larger on the left) in the medial temporal area, next to cranial nerve III. Abbreviations: B = basilar artery, M = medulla, MB = mammillary bodies, OB = olfactory bulb, OC = optic chiasm, ON = optic nerve, TP = temporal pole, V = vertebral artery, and III = cranial nerve III (oculomotor nerve). White arrowheads point to

posterior temporal artery on both right and left. Dashed white lines illustrate atrophy in the cerebellum. Note the black surgical clip on right temporal lobe. [Color figure can be viewed in the online issue, which is available at wileyonlinelibrary.com.]

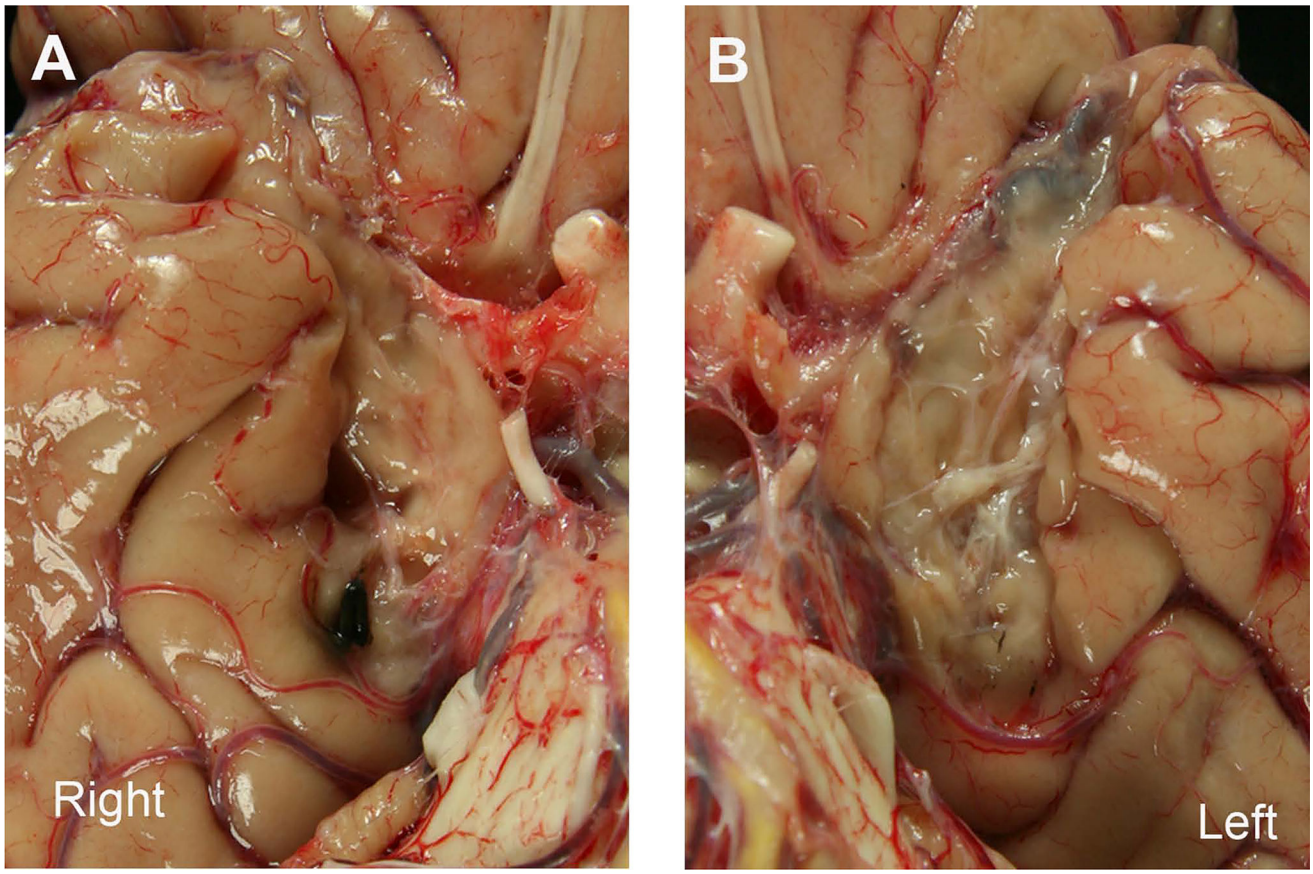

FIGURE 3.

Close-up photographs of H.M.'s medial temporal lobe showing a ventral view of the right and left temporal regions (A and B). Tissue was splayed out (due to being unfixed) to reveal a slightly different viewpoint of the extent of the lesion. In A and B, the lesion extends from the temporal pole to the midparahippocampal gyrus. Note the absence of tissue and the abundant scar tissue bilaterally. The basilar and vertebral arteries contain several atherosclerotic plaques. [Color figure can be viewed in the online issue, which is available at wileyonlinelibrary.com.]

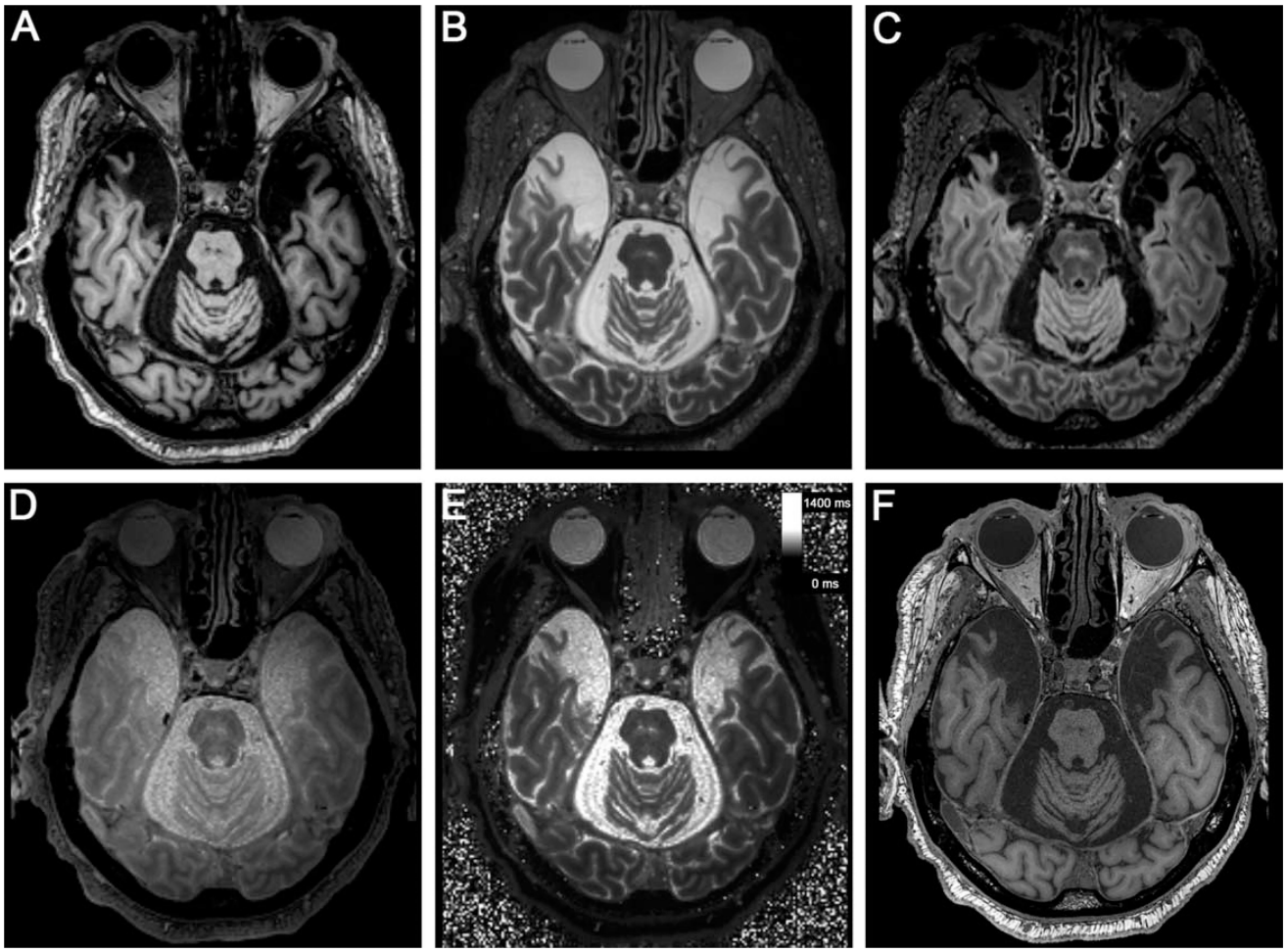

FIGURE 4.

Various MRI contrasts acquired at 3.0 T in situ. (A) multiecho MPRAGE (MEMPR), (B) T2-SPACE, (C) T2-SPACE FLAIR, (D) quantitative PD, (E) quantitative T1, (F) synthetic FLASH. Note the lesion in all contrasts, with the borders especially clear in the multiecho MPRAGE and synthetic FLASH images. T1 and T2-SPACE FLAIR revealed scar tissue faintly in addition to the lesion.

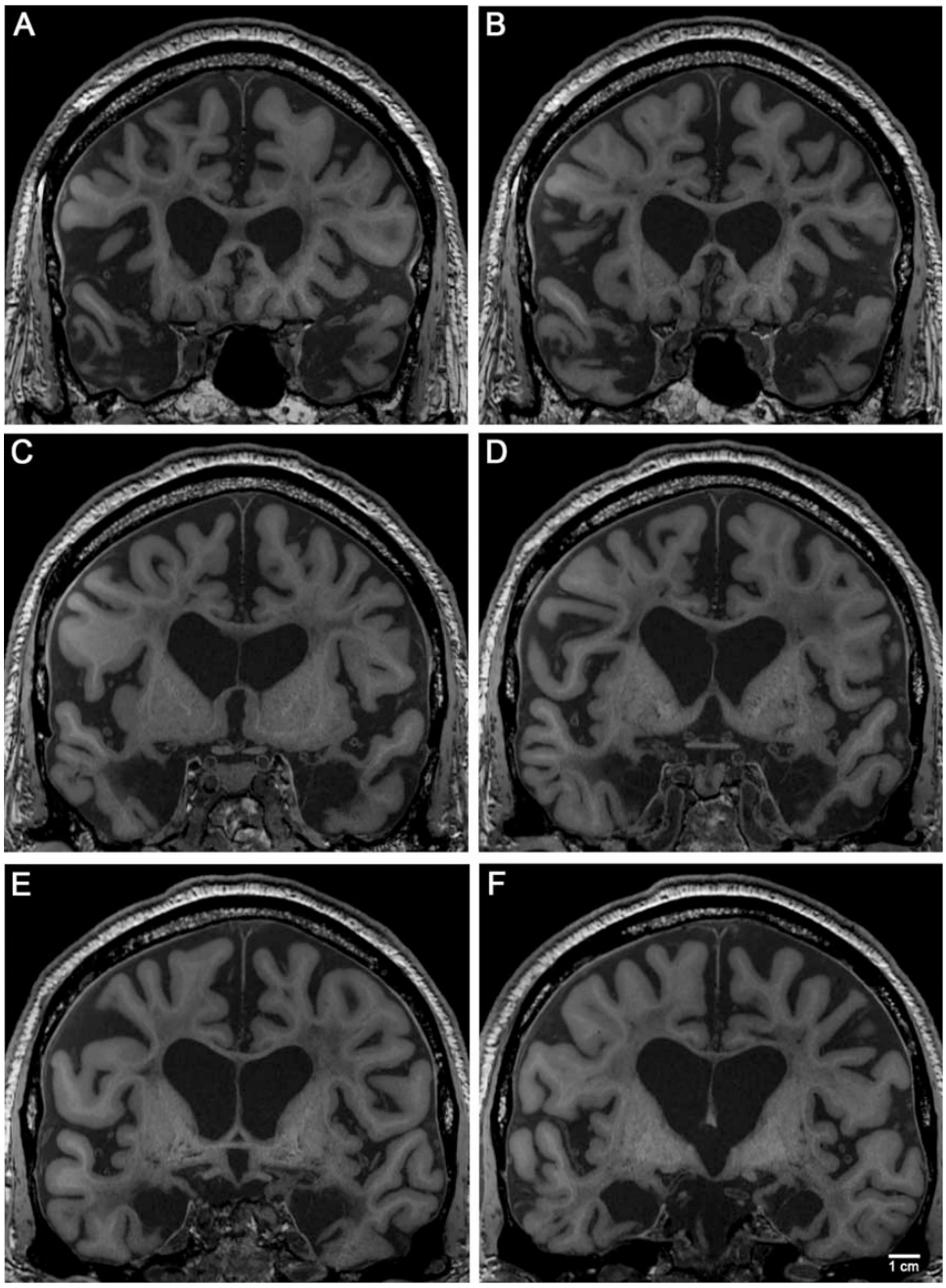

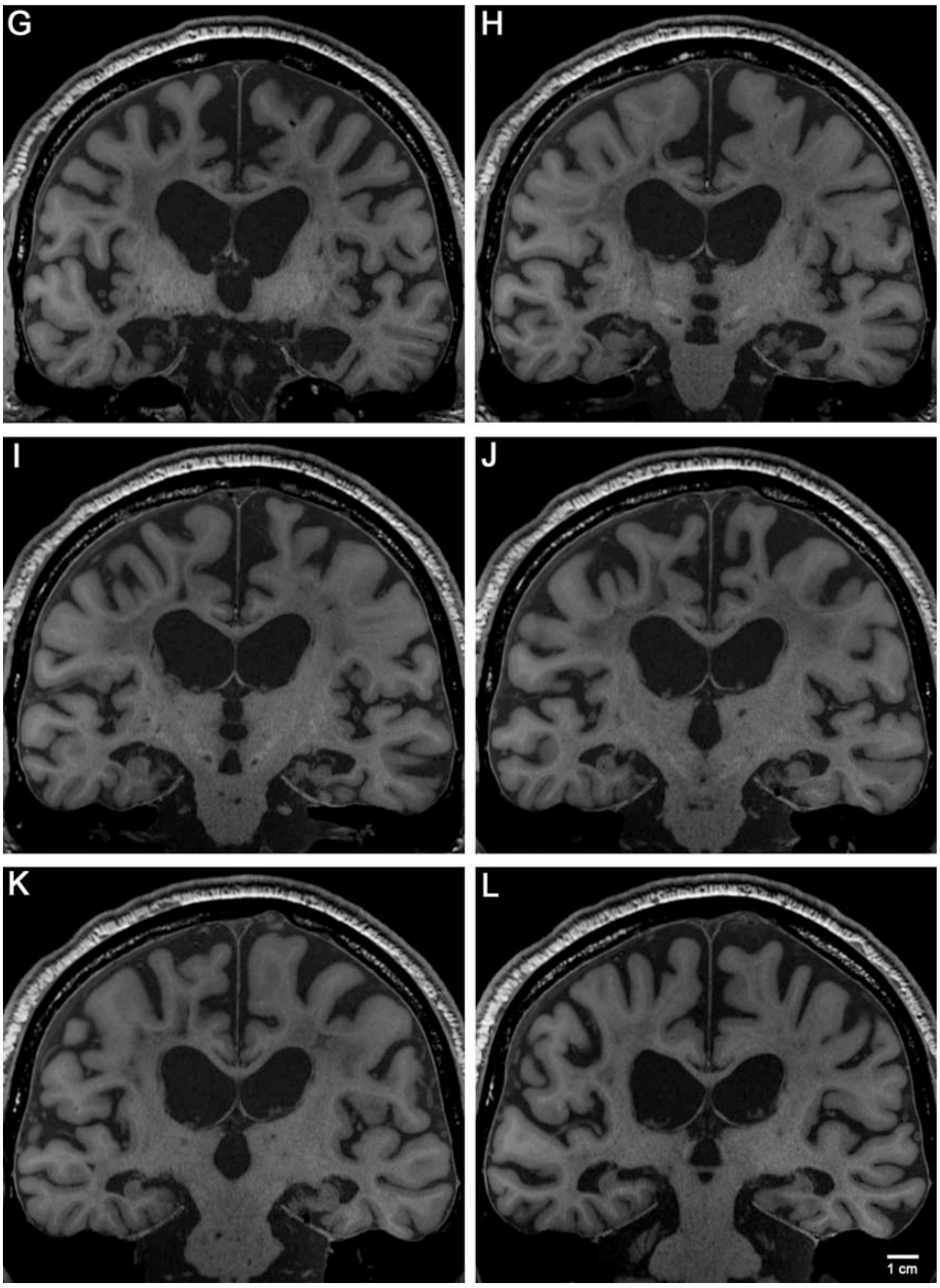

FIGURE 5.

Twelve coronal MR images showing the anterior and posterior extent of H.M.'s medial temporal lobe lesion. Images were synthesized from multi-echo FLASH scans acquired in situ and are ordered from anterior (A) to posterior (L). In all images, note the enlarged ventricles, general atrophy, and a plethora of regional white matter signal abnormalities. We identify particular structures (present or absent) in each panel. A, B, C: medial temporal pole removed; D: anterior entorhinal cortex removed (i.e. piriform cortex), E: cortical amygdala and possibly central nucleus remained; F: gyrus ambiens or uncus remained; G and H: perirhinal cortex and damaged parahippocampal cortex; I: the body of the hippocampus

visible; J: first full observation of parahippocampal cortex (right side) and fimbria; K: posterior tip of the lesion (right side is past the lesion), and L: the undamaged parahippocampal cortex posterior to the lesion. Magnification bar = 1 cm.

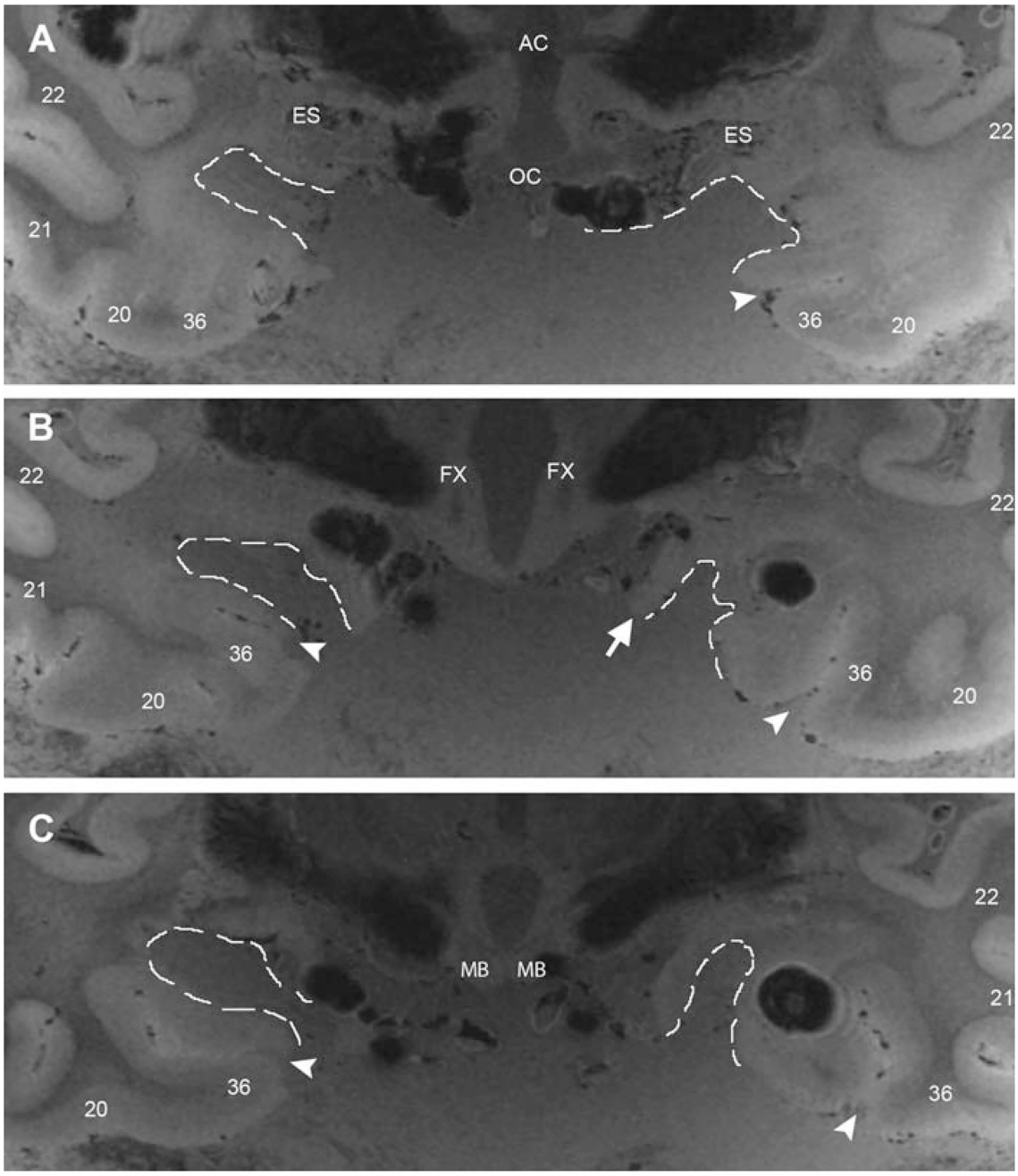

FIGURE 6.

Ex vivo images of medial temporal lobe areas acquired at 7 T. Images at 210 μm isotropic show the extent of the lesion and remaining medial structures. For level-of-cut cross reference, see Figure 5. Panels A, B, and C correspond to the MRI slices in Figures 5E–G. A shows H.M.'s lesion approximately at the level of the amygdala. The lesion shape is relatively uniform at this level. Note the square corners at the dorsal-most part of the lesion. B demonstrates the lesion where the posterior amygdala-anterior hippocampal level would have been. Note the fornix columns medially in the hypothalamus and the irregular lesion shape. The large round black structures in C are regions of susceptibility surrounding air

bubbles. C illustrates the lesion at the level of the mammillary bodies where the head of the hippocampus (i.e., pes hippocampus) would normally reside. At level C the lesion narrows. The shape of the lesion changes considerably from anterior to posterior, scar tissue is visible. The white arrowheads point to the collateral sulcus. Numbers represent Brodmann areas. Abbreviations: AC = anterior commissure, ES = endorhinal sulcus, FX = fornix, MB = mammillary bodies, OC = optic chiasm, RN = red nucleus, and SN = substantia nigra.

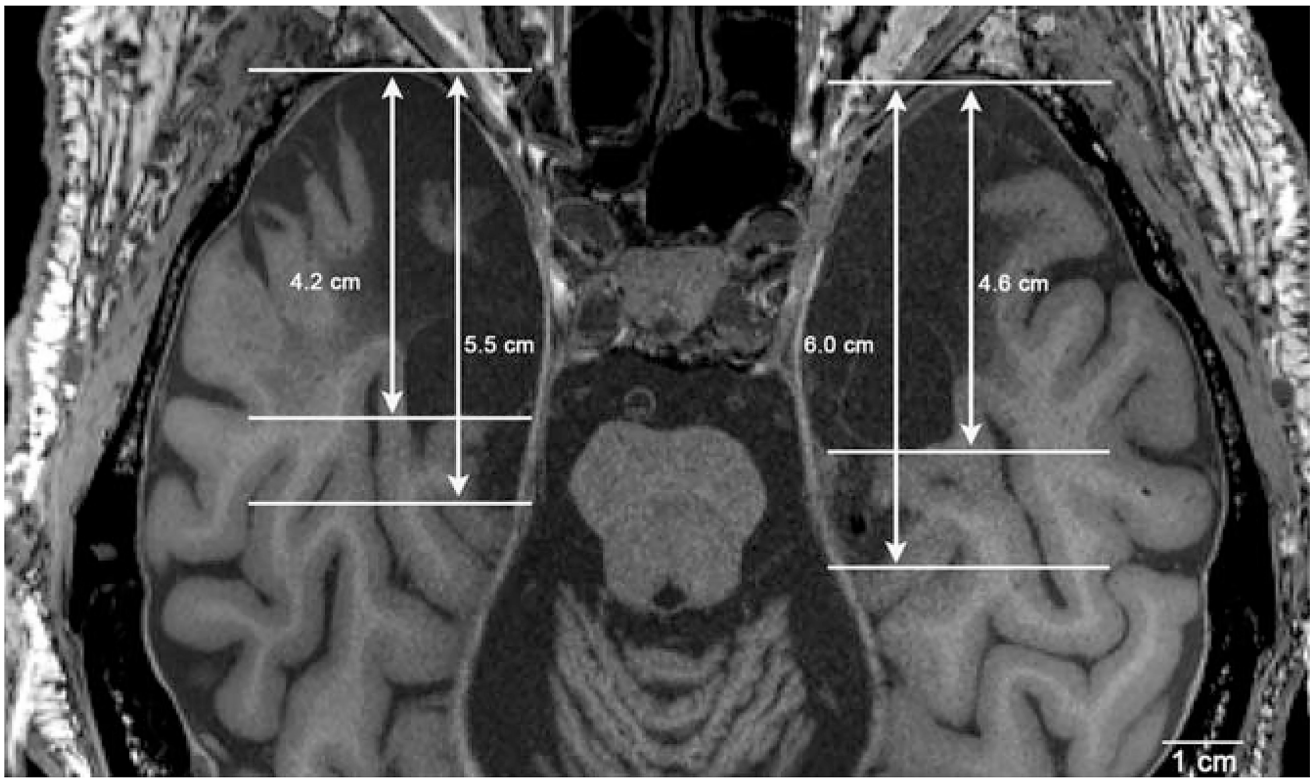

FIGURE 7.

Axial view of the multiecho FLASH images. Line measurements were acquired in the axial plane to assess the anterior-posterior lesion size. The ablation on the right side measured 5.5 cm while the left measured 6.0 cm. The left temporal lobe lost considerably more cortex during surgery. Note the cerebellar atrophy due to Dilantin.